NAG 3-85

CRinc

THE UNIVERSITY of KANSAS CENTER FOR RESEARCH, INC.
2291 Irving Hill Drive-Campus West
Lawrence, Kansas 66045

FINAL REPORT

AN ANALYSIS OF CROSS-COUPLING OF A MULTI COMPONENT JET ENGINE TEST STAND USING FINITE ELEMENT MODELING TECHNIQUES

by

William G. Schweikhard and Werachone N. Singnoi

University of Kansas Center for Research, Inc.

prepared for

National Aeronautics and Space Administration
NASA Lewis Research Center
NASA Contract No. NAG 3-85

SUMMARY

The development of thrust vectoring nozzles for airbreathing propulsion systems requires the development of test facilities that can measure thrust along all three orthogonal axes of the engine. The design and analysis tools for developing systems capable of making these measurements are in an emerging state.

An analysis of a two axis thrust measuring system has been done using a finite element computer program to determine the sensitivities of the system to misalignment of the load cells and applied loads, and the stiffness of the structural members. Three models were evaluated: 1) The basic measuring element and its internal calibration load cells; 2) The basic measuring element and its external load calibration equipment; and 3) The basic measuring element, external calibration load frame and the altitude facility support structure. Comparisons were made with experimental data.

Alignment of calibration loads was found to be the greatest source of error for multi-axis thrust measuring systems. Uniform increases or decreases in stiffness of the members, which might be caused by the selection of the materials, was found to have little effect on the accuracy of the measurements. The POLO-FINITE program was found to be a viable tool for designing and analyzing multi-axis thrust measurement systems.

A preliminary dynamic analysis of the test stand was done to determine the response of the test stand to step inputs that might be encountered with thrust vectoring tests. The dynamic analysis showed a potential problem for measuring the dynamic response characteristics of thrust vectoring systems because of the inherently light damping of the test stand. Further investigations are required in this area.

TABLE OF CONTENTS

LIST OF FIGURES

1.0 INTRODUCTION

Thrust vectoring has been used extensively for rocket engines in space applications. In these applications vectoring has been accomplished by gimbaling the entire engine or by fluid injection into the nozzle. These solutions cannot be used in airbreathing engine applications because of both the long duration of operation that is required and because the inlet section of the engine must remain fixed relative to the airframe. Therefore, only the nozzle can move. The vectoring solutions for airbreathing engines have gravitated toward the two dimensional rectangular nozzles that can function primarily in the pitch axis of the airplane. In this mode the vectored nozzle can provide pitch trim and active pitch control thus reducing the size, weight and trim drag contribution of aerodynamic surfaces and controls.

If thrust vectoring is to be the technology of the future, there is a need to be able to test and develop these nozzles in sea level and altitude test facilities. The measurement of the components of thrust in more than one axis is required. A literature search (Ref. 1) was conducted and indicated that there is little capability for measuring side components of thrust for vectored airbreathing engines, nor are the analytical tools available for designing and analyzing thrust stands having multi-axis thrust measuring capabilities (i.e., three components of thrust and moments along or about the three orthongonal axes).

The purpose of this investigation was to evaluate finite element computer modeling as an analytical tool for design and analysis of test stands of this type. Finite element information used in this study is contained in References 2 through 8. The test stand selected was a new two-component Ormond test stand for use in the Propulsion Simulation Laboratory (PSL) facility at NASA Lewis Research center. The two-component Ormond test stand is capable of measuring axial and side force only, however the principles developed here can be applied to more complex systems.

This report presents a detailed description of the Ormond test stand and its calibration. The finite element modeling technique is described along with specific applications for static structural analyses of three models. The three models analyzed were the Ormond test stand with its internal calibration devices, the Ormond test stand with external calibration fixtures, and the complete PSL facility consisting of the Ormond test stand, calibration fixtures and the NASA supporting structure of the facility. Comparisons of

the analytical results were made with the experimental results to verify the analysis.

The model of the Ormond test stand was developed to examine the accuracy and sensitivities caused by internal interaction characteristics of the test stand. Since this did not explain experimental discrepancies that had been observed, two additional models were developed to examine more of the total facility support structure.

A preliminary dynamic analysis of the test stand was also included in this study. The analysis points out various mathematical models of load cell response problems during step and cyclic thrust vectoring operations.

2.0 METHOD OF ANALYSIS

There are two parts to the analysis presented in this report. The first is the description of the Ormond test stand and calibration method. The second is discussion of the method and the finite element model used in the static structural analysis.

2.1 Ormond Test Stand

The Ormond designed test stand for airbreathing jet engines at the NASA Lewis PSL facility can be used to measure axial thrust and side force in a plane. The maximum axial capacity is 30,000 pounds and the side-force capacity is 10,000 pounds.

2.1.1 General Characteristics

Figure 1 is a photograph of the total apparatus in the two-component test stand mounted on the PSL test cell structure in preparation for simulating engine centerline calibration. A schematic of the total system shown in Figure 2 identifies the major components analyzed in this study. A three-view drawing of the Ormond test stand and an isometric view of the Ormond test stand structure is shown in Figures 3 and 4 respectively. The test stand has a rectangular shape and consists of an upper and lower structure. The upper structure, or ground frame, is the stationary component and is attached to the PSL test cell structure. The lower structure, or the live bed, is connected to the ground frame by means of vertical struts with universal flexures at the four corners of the test stand.

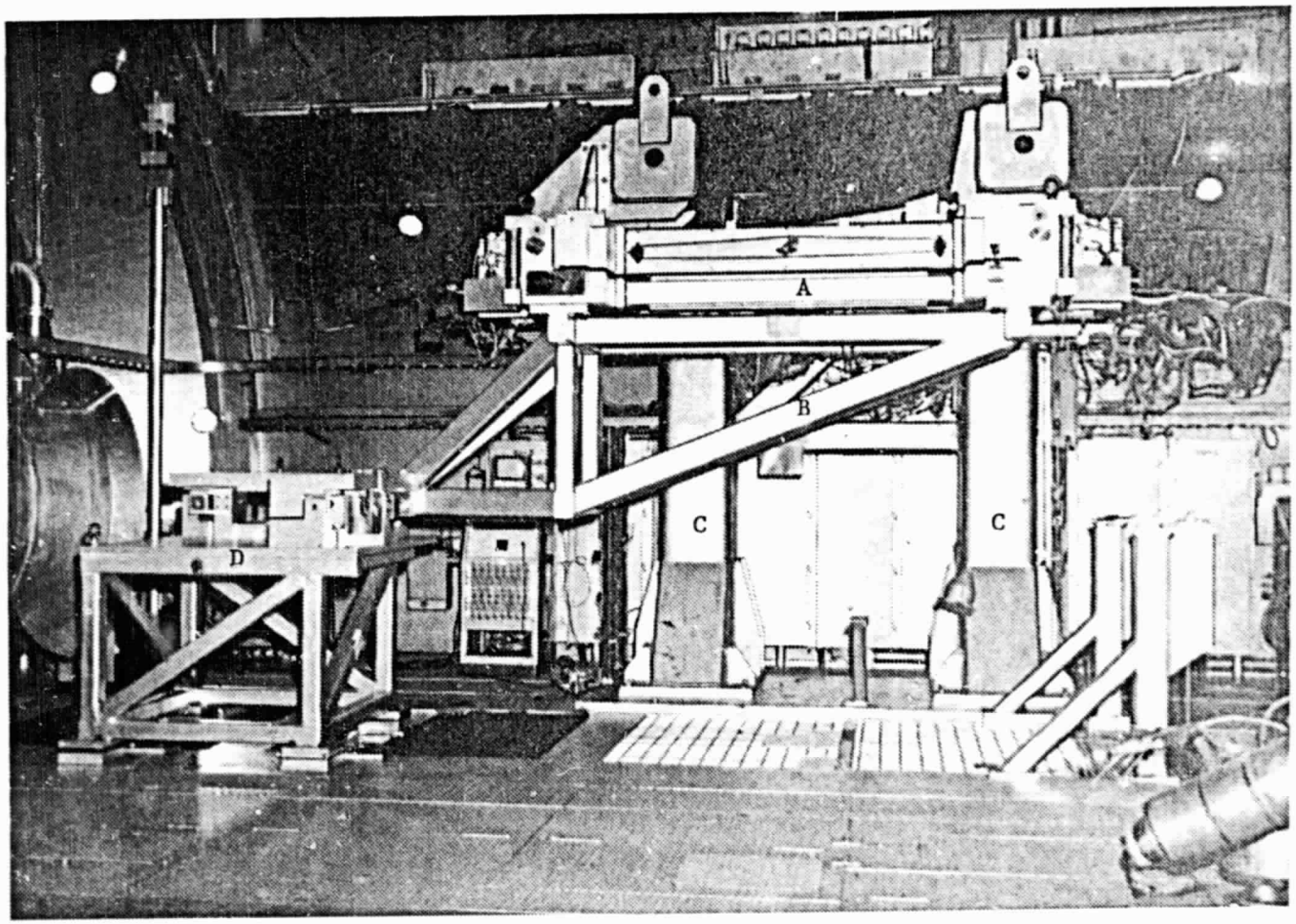

Figure 1. Picture of Ormond Test Stand and External Calibration Rig Mounted in PSL Test Cell

COMPONENTS:
- A. ORMOND TEST STAND
- B. SIMULATED ENGINE CENTERLINE CALIBRATION FRAME
- C. ENGINE MOUNT
- D. ENGINE CENTERLINE CALIBRATION SUPPORT FRAME

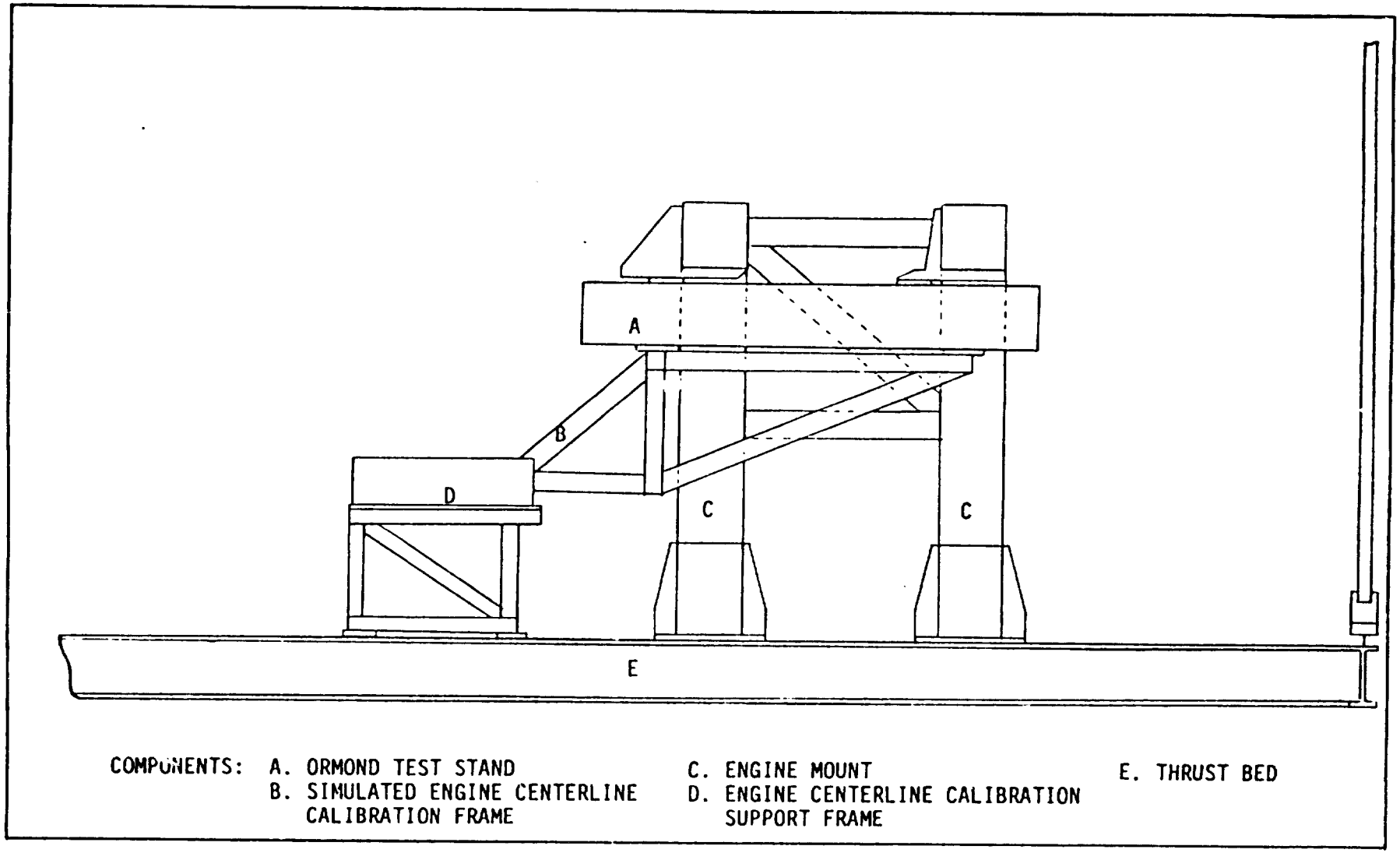

Figure 2. Schematic View of Overall PSL Facility and Ormond Test Stand with Calibration Frames Attached

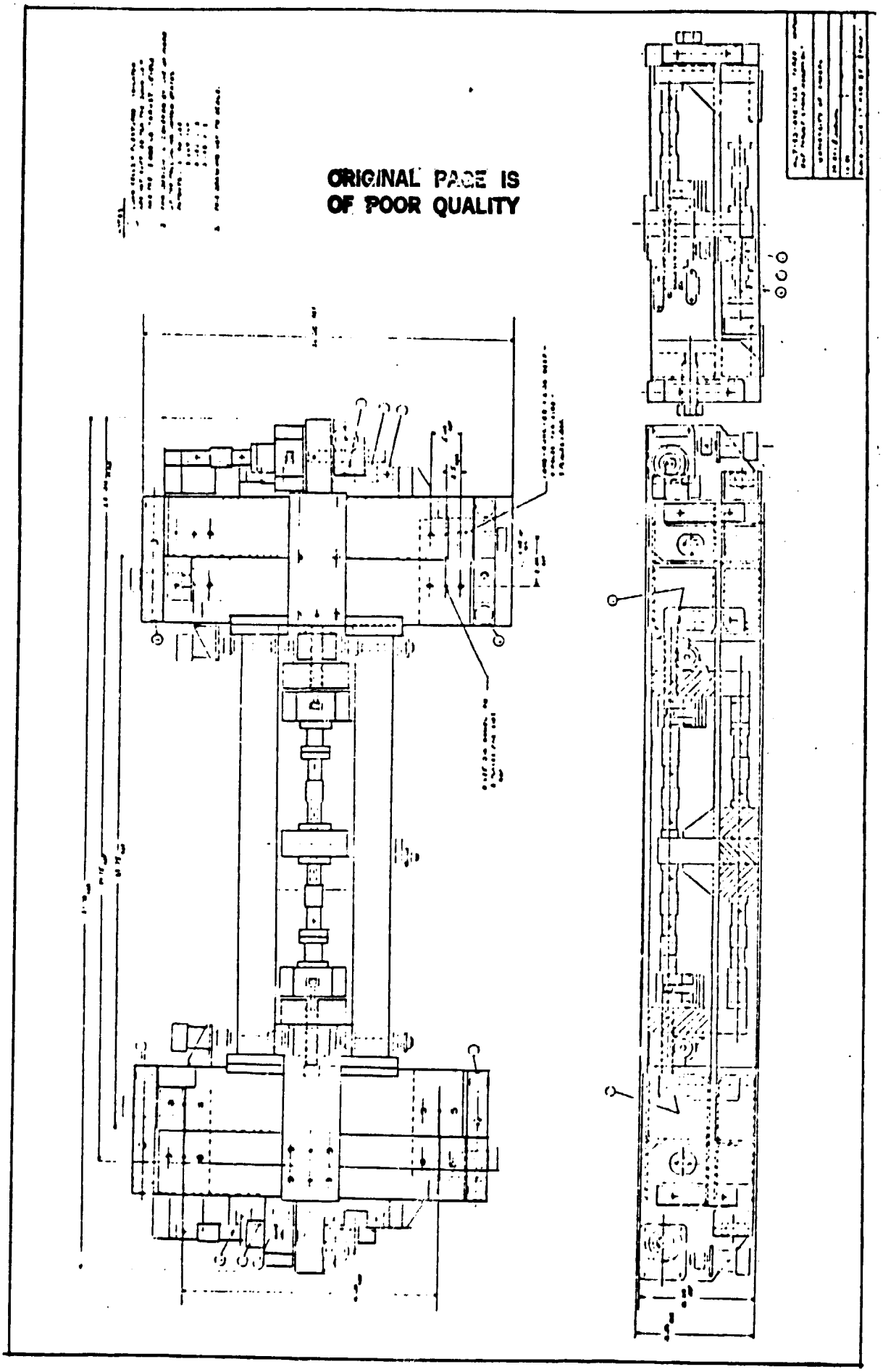

Figure 3. Three Views - Drawing of Ormond Test Stand

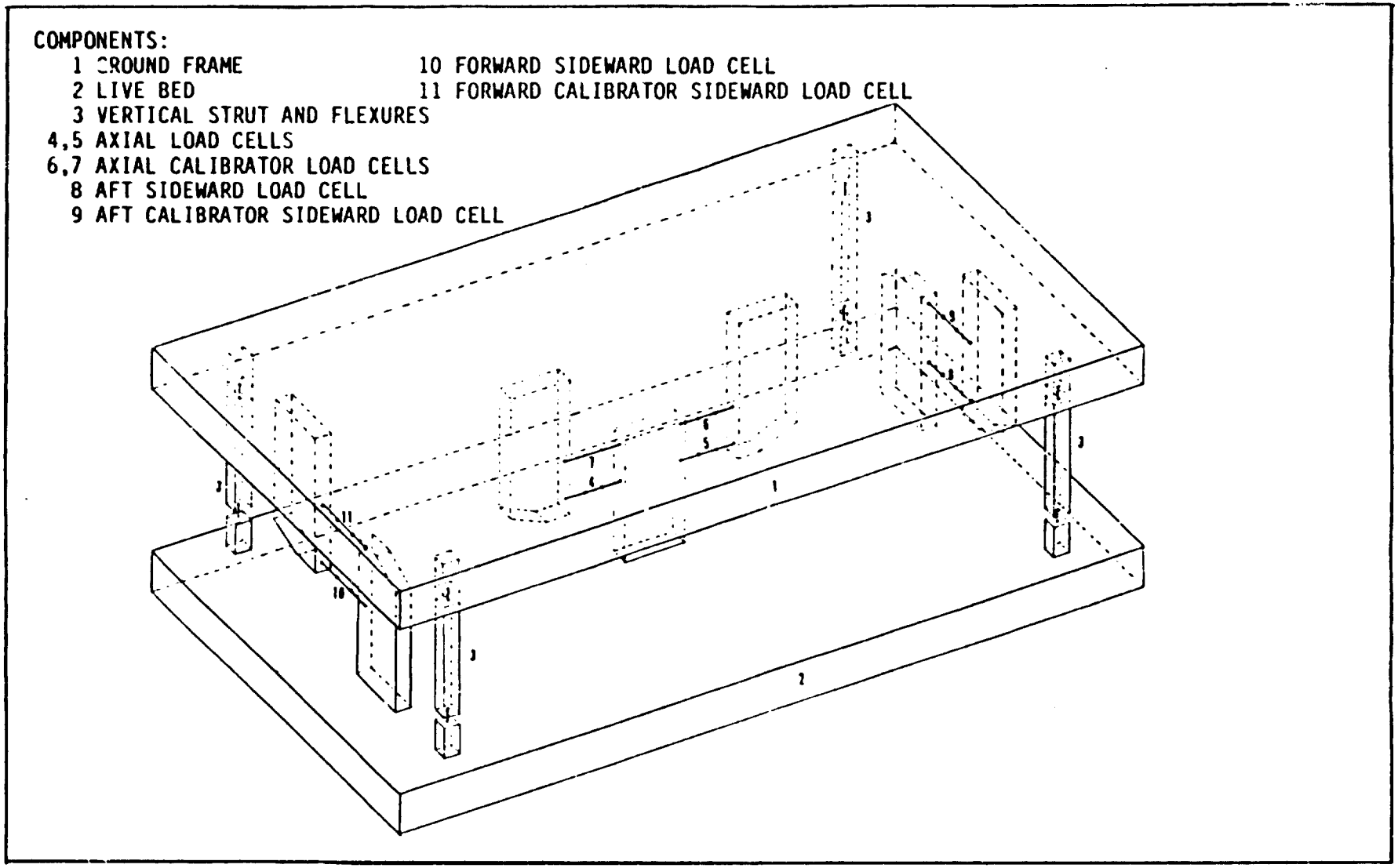

Figure 4. Schematic View of Ormond Test Stand

As seen in Figures 3 and 4 the test stand consists of four pairs of load cells, one above the other. Two pairs are located along the test stand centerline, a pair located laterally at the forward end and another pair at the rear of the test stand. The upper load cell of each pair is used as a built-in calibration system. They are disconnected during actual testing thus allowing the reaction forces to be read from the lower load cells. The load cells located along the test stand centerline measure the axial component of the principle thrust force. The two lower centerline load cells are arranged such that the load sensitive axes of the two load cells are located in line with each other and parallel to the direction of axial thrust force. This arrangement causes one of the load cells to be in compression in response to a principle thrust force and the other load cell in tension. As a result of this arrangement, any side force components of the principle thrust force result in the generation of interacting side forces in opposite directions which substantially cancel each other. The load cells located laterally at front and rear of the test stand measure the side force component of the principle thrust force.

The Ormond test stand is a specially designed compact measuring system. The test stand is of modular construction, which allows complete assembly and check-out before installation. Thus, the measuring system can be manufactured, calibrated, and shipped as a module and installed without requiring complex assembly and alignment. After installation, the engine likewise can be installed and removed without affecting the test stand alignment. Special design configurations and techniques are incorporated in the thrust measuring system in order to minimize error terms.

2.1.2 Calibrations

Thorough calibrations are essential to the realization of a highly accurate force measurement system. The Ormond test stand was designed to be readily calibrated either by a built-in calibration system or by a special external calibration rig that simulates forces at the engine centerline.

After initial alignment, the test stand was first calibrated using the built-in calibration system. The built-in calibration system consists of a hydraulic screw jack that is aligned with each upper (calibration) load cell. During the internal calibration, a screw jack applied a known force, read from the upper calibration load cell, to the test stand, and the

resultant forces were read directly from the lower (test) load cells. The calibration forces ranged from -15,000 to +15,000 pounds of axial force, and -5,000 to +5,000 pounds of side force at sea level condition. The calibration data were obtained from the NASA Lewis Research Center.

A second calibration was done using an external calibration frame that simulates loads applied off center at a typical engine centerline location. Figure 1 shows the test stand with the external calibration engine centerline frames designed by Ormond Inc. (Components B & D). The same calibration force increments as those used in the previous built-in calibration were applied. However, unexpected defections were observed between components B and D of Figure 2. During the external calibration process, an average displacement of .375 inches was observed when a simulated engine axial thrust of 10,000 pounds was applied. This deflection was considered excessive and the cause needed to be identified and corrected. Because of the complexity of the test apparatus a sophisticated finite element analysis was employed to pinpoint this problem and to evaluate its use as a design tool for future designs.

2.2 Static Structural Analysis

A static structural analysis was done using the finite element computer modeling method. The method used in this study was developed by the University of Illinois at Urbana-Champaign and operates under control of the POLO II data base management system. This system is operational on the Honeywell computer at the University of Kansas.

FINITE is a general-purpose computer program for the stress analysis of structures and mechanical systems subjected to various types of static loading. The program executes under control of Problem Oriented Language Organizer (POLO) engineering supervisory system. It also has an integrated graphic subsystem capable of providing accurate color visual representation of a full 3-dimensional structure. References 2 and 3 can be consulted for more detailed information about the FINITE system.

FINITE utilizes finite element stress analysis. The finite element method divides a continuous structure into a series of elements interconnected by discrete nodal points. Each element type has its own interpolating shape function to describe the variation of displacements. Derivatives of the element shape functions and nodal displacements define the state of strain within the element. Individual element stiffness matrices are formulated by

the principle of virtual displacements or minimum potential energy. Based on the interconnection of the elements, individual element stiffness matrices are combined to form a large stiffness matrix for the overall structure. This stiffness matrix is used to solve for the unknown nodal displacements, which are then used to compute the stress and strain for each element.

2.2.1 Development of FINITE Element Models

The purpose of developing the finite element model was to assist in interpreting the test results for the Ormond test stand and for identifying the source of the unexpected defection in the test apparatus. If done successfully this would demonstrate the utility of the POLO FINITE program as a design tool for future, more complex multi-axis thrust measuring systems, for example, a 6-component system (3-axis forces and 3-axis moments).

Three separate models were developed in this investigation. Model I, II, and III were represented by simple 3-D rigid space frame structures. Model I was a rigidly supported Ormond stand (Fig. 2, element A). Model II was a rigidly supported Ormond stand plus element B of Figure 2. Model III included all of the NASA test facility supporting structure. Each of the models will be described in detail including the topology, loading conditions, and constraints of each. Structural definitions, idealizations, and assumptions are also discussed.

2.2.2 General Structural Definitions for Application of Finite Element Analysis

FINITE accepts user input data in a form of problem oriented language commands (statements). The syntax and acceptable options for individual commands are described in Reference 3. A summary of required and optional data classes to define a structure are listed.

Required Commands:

1. Initiate the definition with the STRUCTURE command and assign a unique name to the structure.
2. Specify the number of nodes, elements, and optionally, the number of coordinate points. These items must be stated immediately after the STRUCTURE command.
3. Define the "type" of each element in the structure either by element characteristics or library elements.
4. Provide incidences for each element relating structure node numbers to element node numbers.

Optional data:

1. Specify coordinates of nodes as necessary.
2. Define boundary conditions via CONSTRAINTS.
3. Define loading conditions.

2.2.3 Idealizations and Assumptions

The first stage of structural analysis is to idealize a proposed actual structural system so that discrepancies between the geometry of actual structure and the idealized model are minimized.

All the structural joints are assumed to be rigid. The structural arrangements are aligned according to design specifications. Note that this assumption is not always the case for actual structures, because misalignment can be induced by minor measurement errors during the manufacturing of the test stand. Some dimensions in the model may not seem to match the actual structural dimensions exactly. It must be kept in mind that the objective is to accurately match the physical characteristics of the actual structure. The weight of structural members is not included in the analysis. The effect of self weight is assumed to be minimal in comparison to the loading conditions. The assumption that the loading condition is small compared to structural strength implies that the computation is linear based upon the usual elastic, static, small displacement and small deformation finite element formulations.

2.2.4 Model I

The structural model of the Ormond test stand is represented by Model I (Figures 4,5). Model I is designed to analyze interaction factors affecting test stand accuracy when it is loaded by a built-in internal calibrator system. Model I is the basic model in the present analysis and becomes a part of more complex analysis in Model II and III.

Referring to Figure 4, Model I assumes that the ground frame is fixed and the metric (live) bed is the only moving and elastic component of the test stand. Figure 5 represents the topology of Model I, which consists of 65 nodes and 58 elements. The center of the global coordinate system is located above node number 1, where x, y, and z define longitudinal, lateral, and vertical axes. Nodes 18, 21, 24, 27, 32, 36, 54, and 58 are fixed, representing stationary ground frame. The matrix bed is represented by inter-connect-

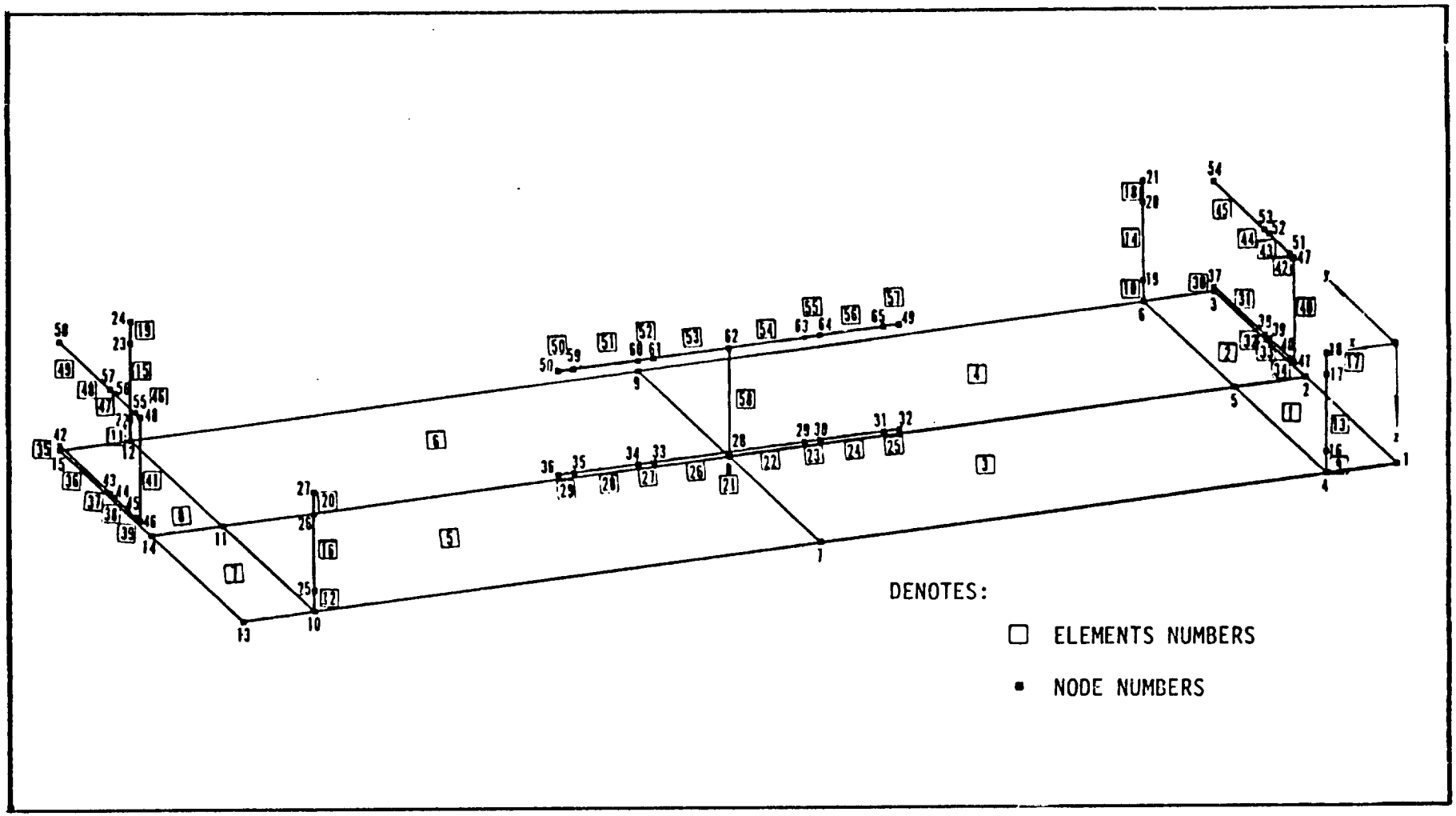

Figure 5. Topology for Model I

ing rigid rectangular flat plates suspended by a combination of vertical struts and universal flexures located above nodes 4, 6, 10, and 12. The axial and sideward load cells are represented by elements 24, 28, 51, 56, and 33, 38, 43, 47. Reference 8 contains load cells and flexures characteristics.

Internal calibration loads represented by nodal loads applied along the centerline of the upper calibrator load cells and measured by lower load cells are based on calibration procedures.

Reference 8 contains sample FINITE element input and output data of Model I. The input consists of structural definitions, nodal coordinates, incidences, constraints, and loading conditions. The output consists of resultant element loads, stresses, and nodal displacements.

2.2.5 Model II

Model II is a combination of Model I and a model of the external calibrator frame. Model II is designed for the analysis of simulated engine centerline calibration. Figures 6 and 7 are a schematic and a detailed three-view drawing of an engine centerline calibrator frame.

The topology of Model II for FINITE analysis is shown in Figure 8. Model II consists of 72 nodes and 75 elements. The external calibrator frame is attached to the test stand (Model I) by rigid joints. Nodal loads representing external calibration loads are applied along the simulated engine centerline at node number 72.

2.2.6 Model III

Model III represents the entire structure of the NASA test facility. It is a combination of Model II plus the PSL structure. The analysis of the PSL facility and test stand integration is base n Model III.

The PSL structure consists of two major components, the engine mount, and the thrust bed structures, represented by Figures 9 and 10. These are identified schematically in Figure 2. Model II is attached to the PSL structures by rigid joints located on the engine mount structure. The external calibration force was applied at the engine centerline calibration support frame (Figures 6 and 11).

The topology of Model III is shown in Figure 12. Note that the topology shows only nodal numbers without accompanying element numbers. This is due to the large and complex structural arrangements. Model III consists of 386

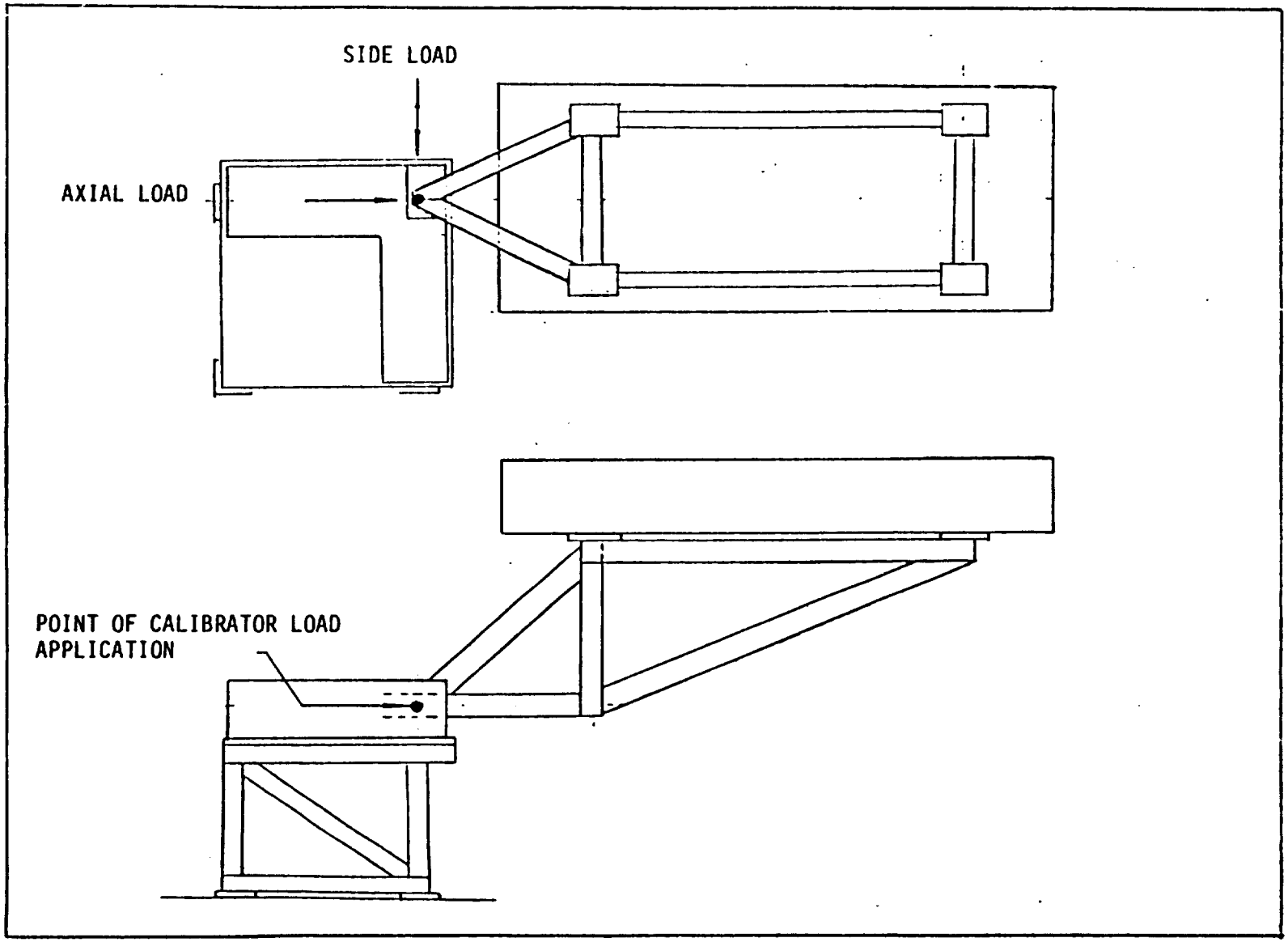

Figure 6. Schematic View of Simulated Engine Centerline Calibration

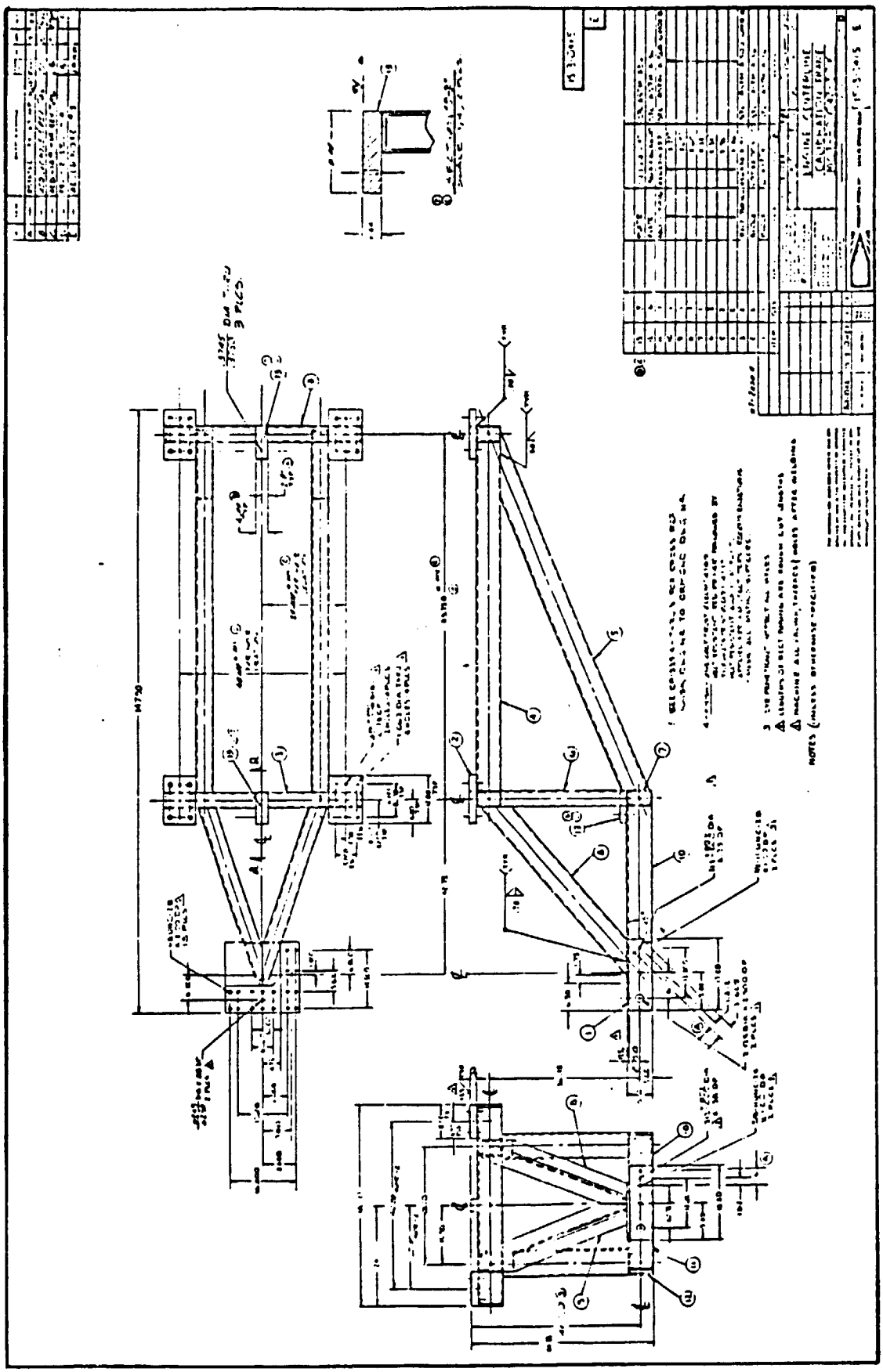

Figure 7. Engine Centerline Calibration Frame

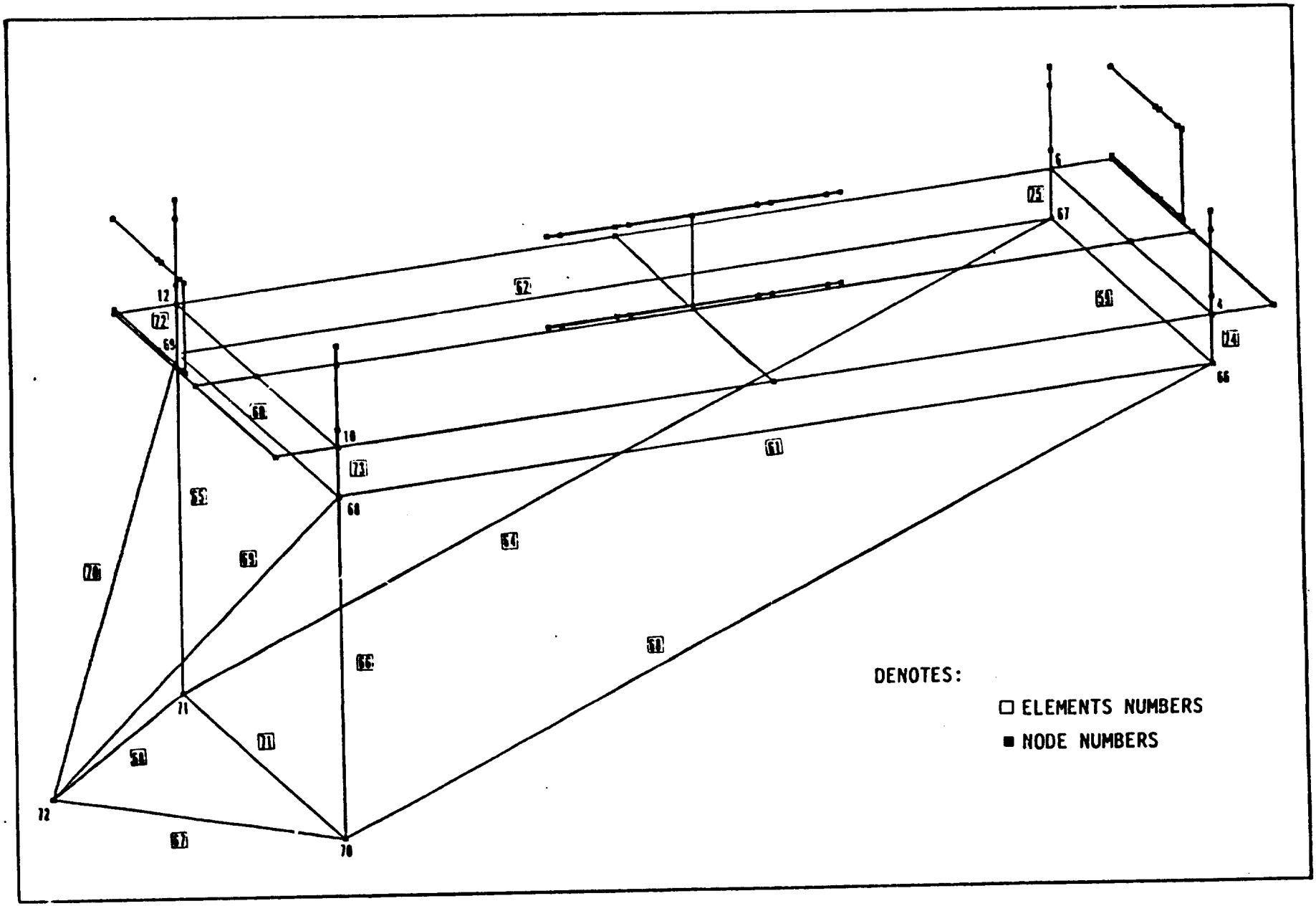

Figure 8. Topology for Model II

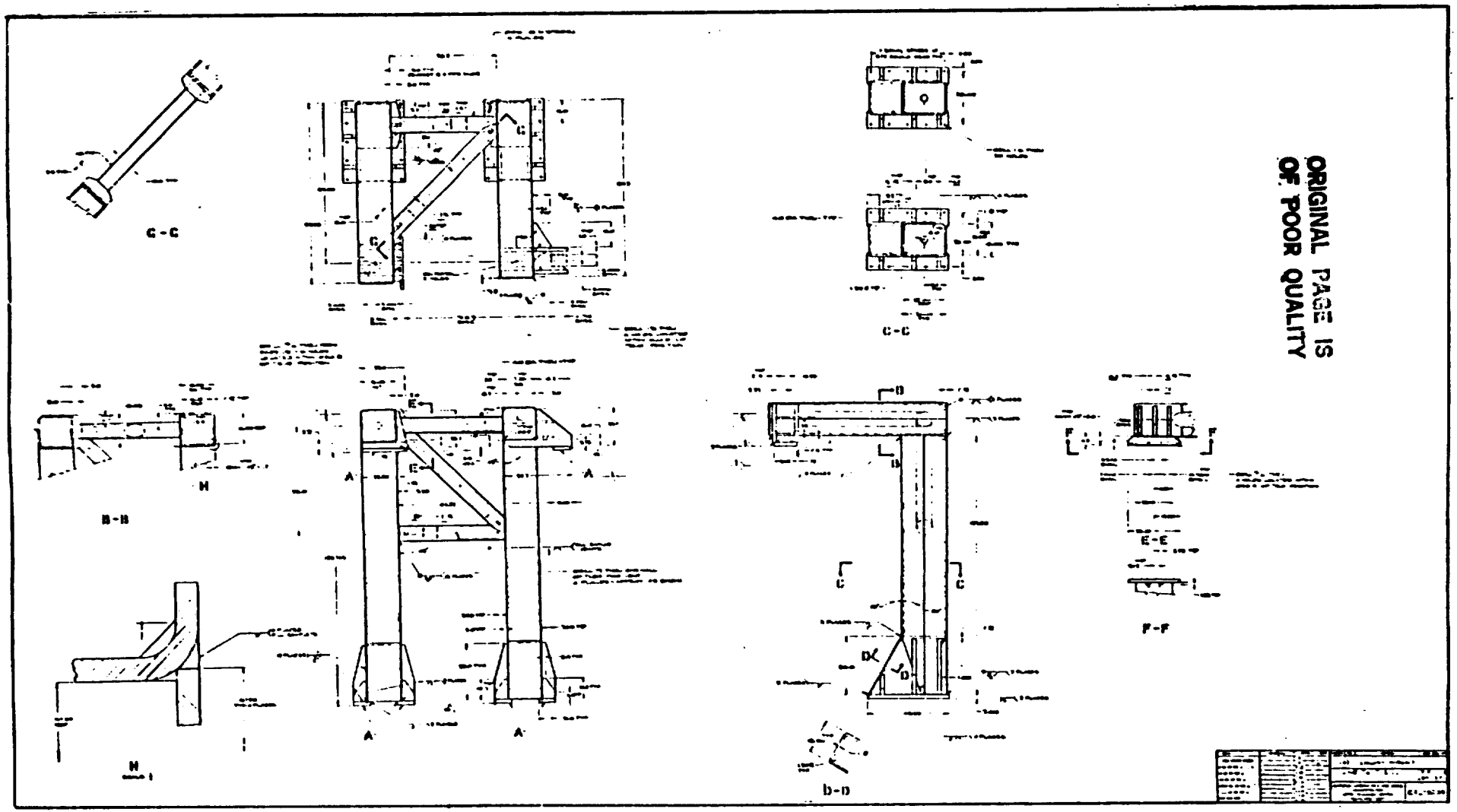

Figure 9. Engine Mount

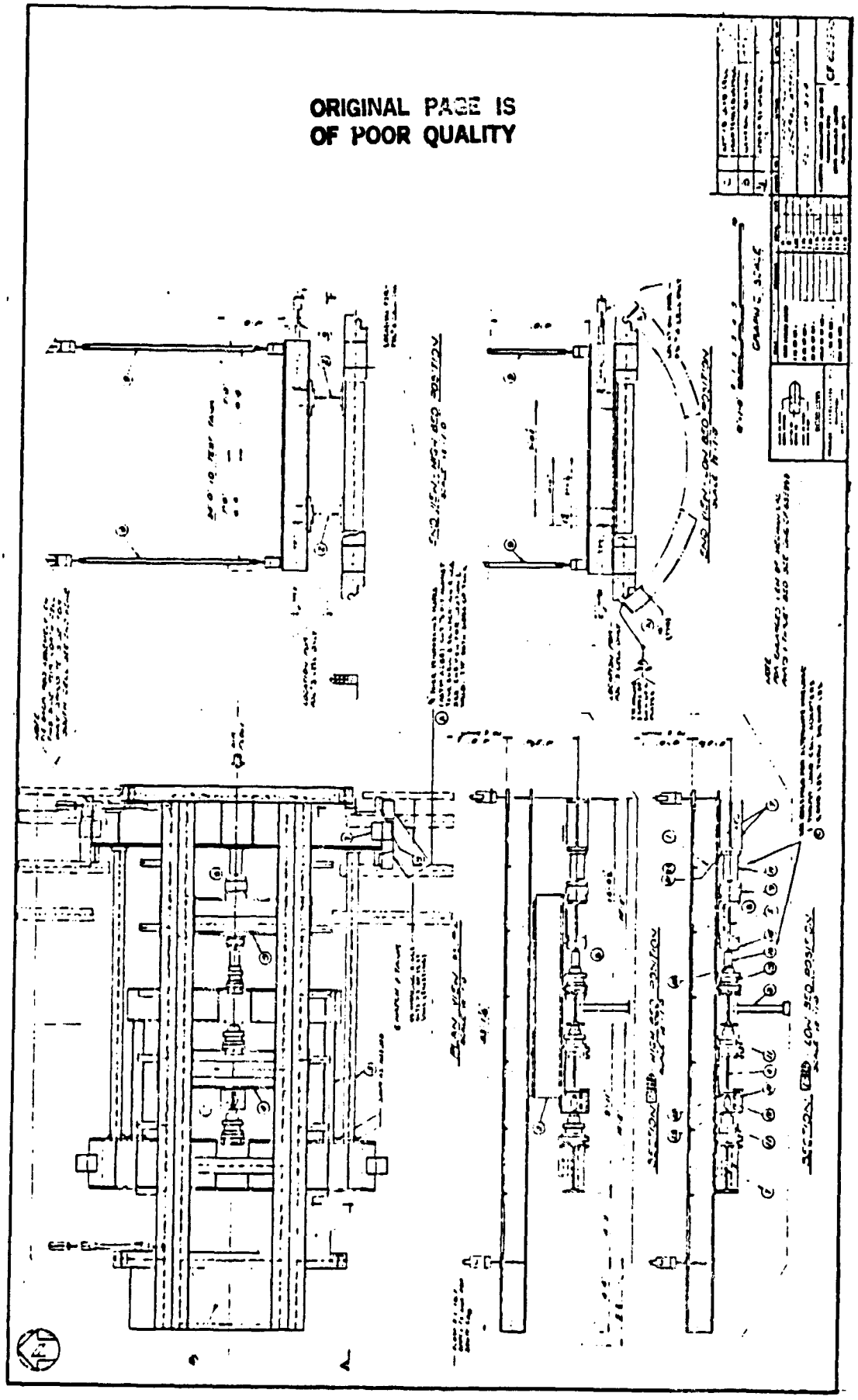

Figure 10. Thrust Bed

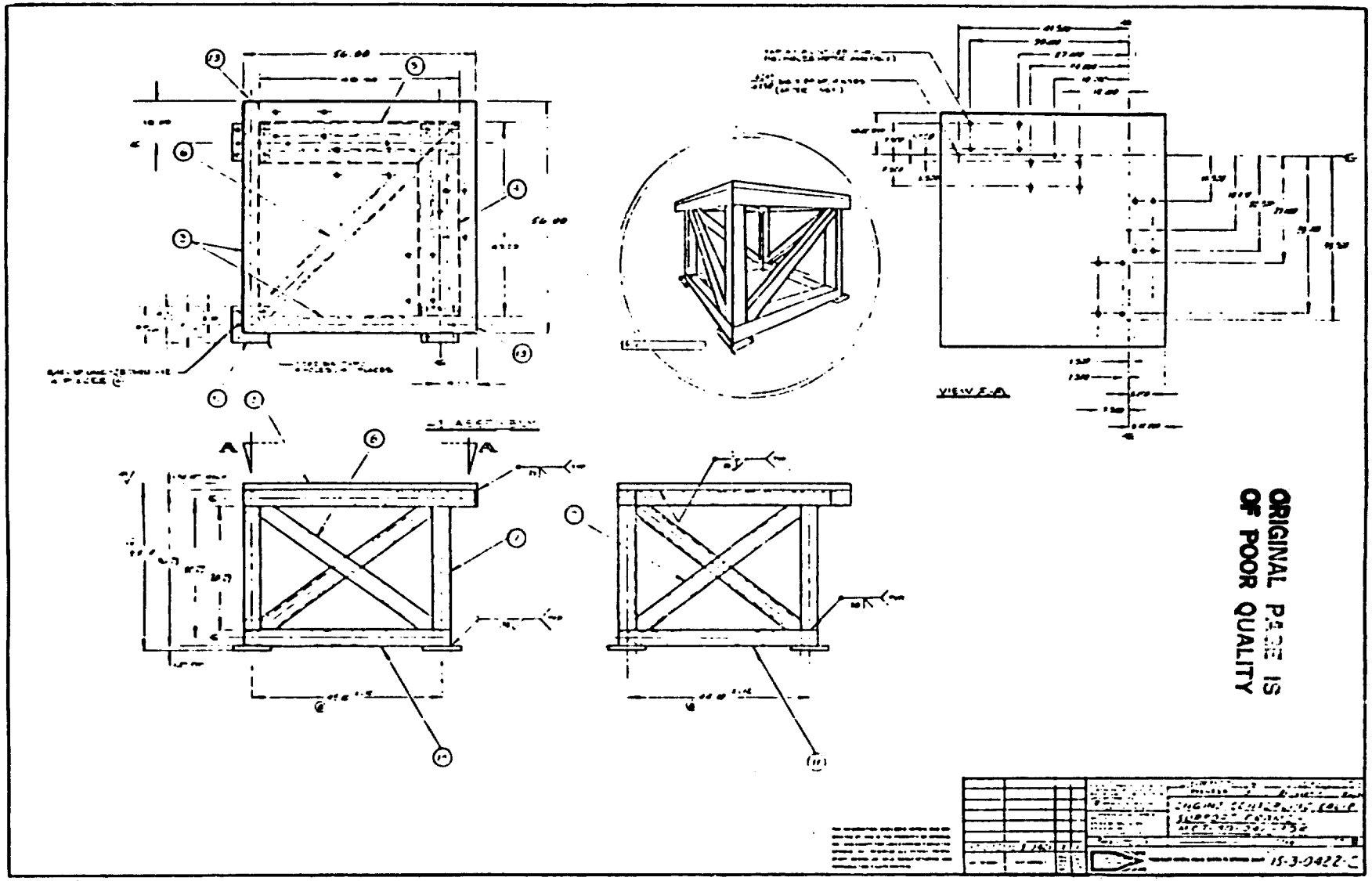

Figure 11. Engine Centerline Calibration Support Frame

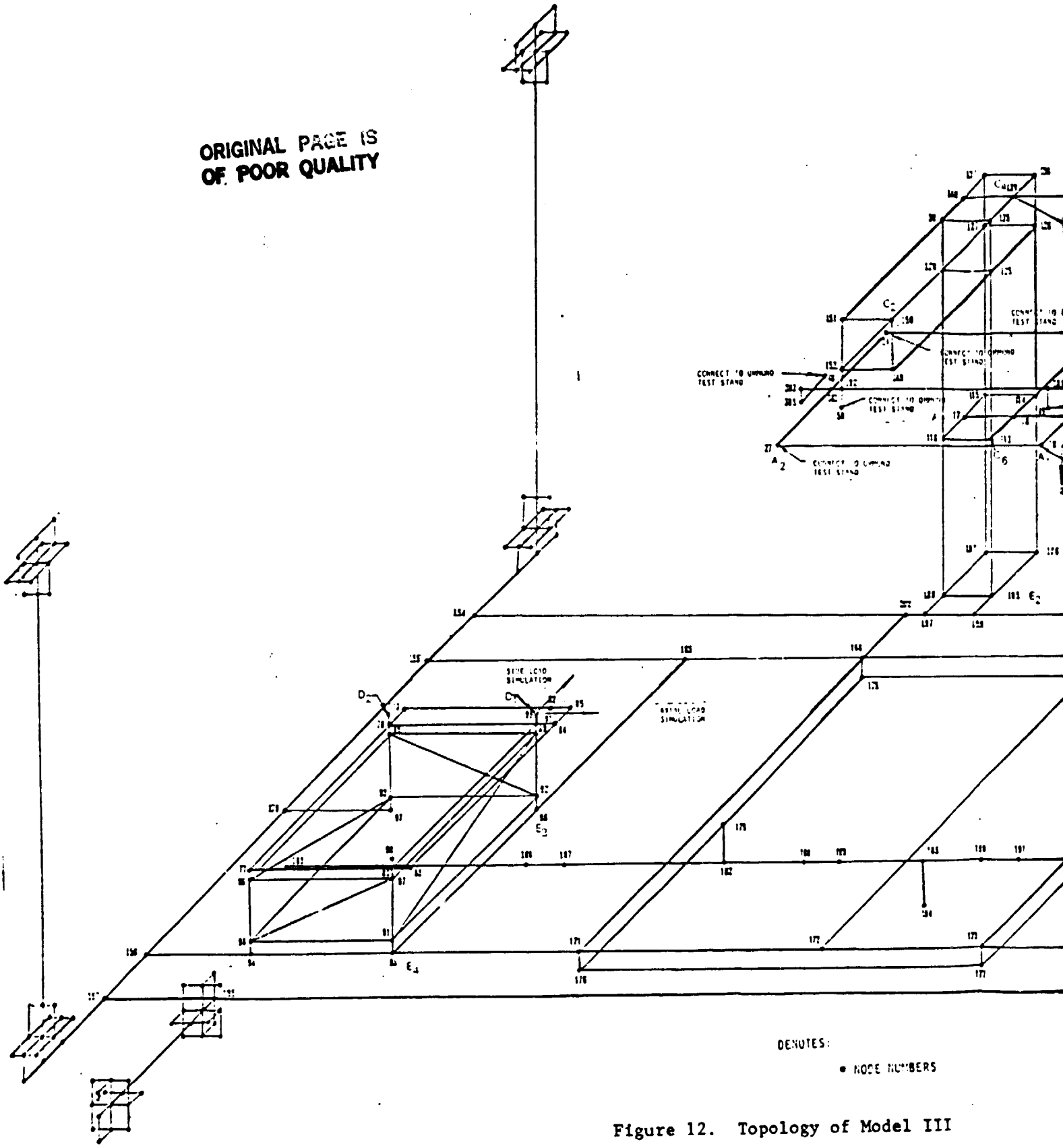

Figure 12. Topology of Model III

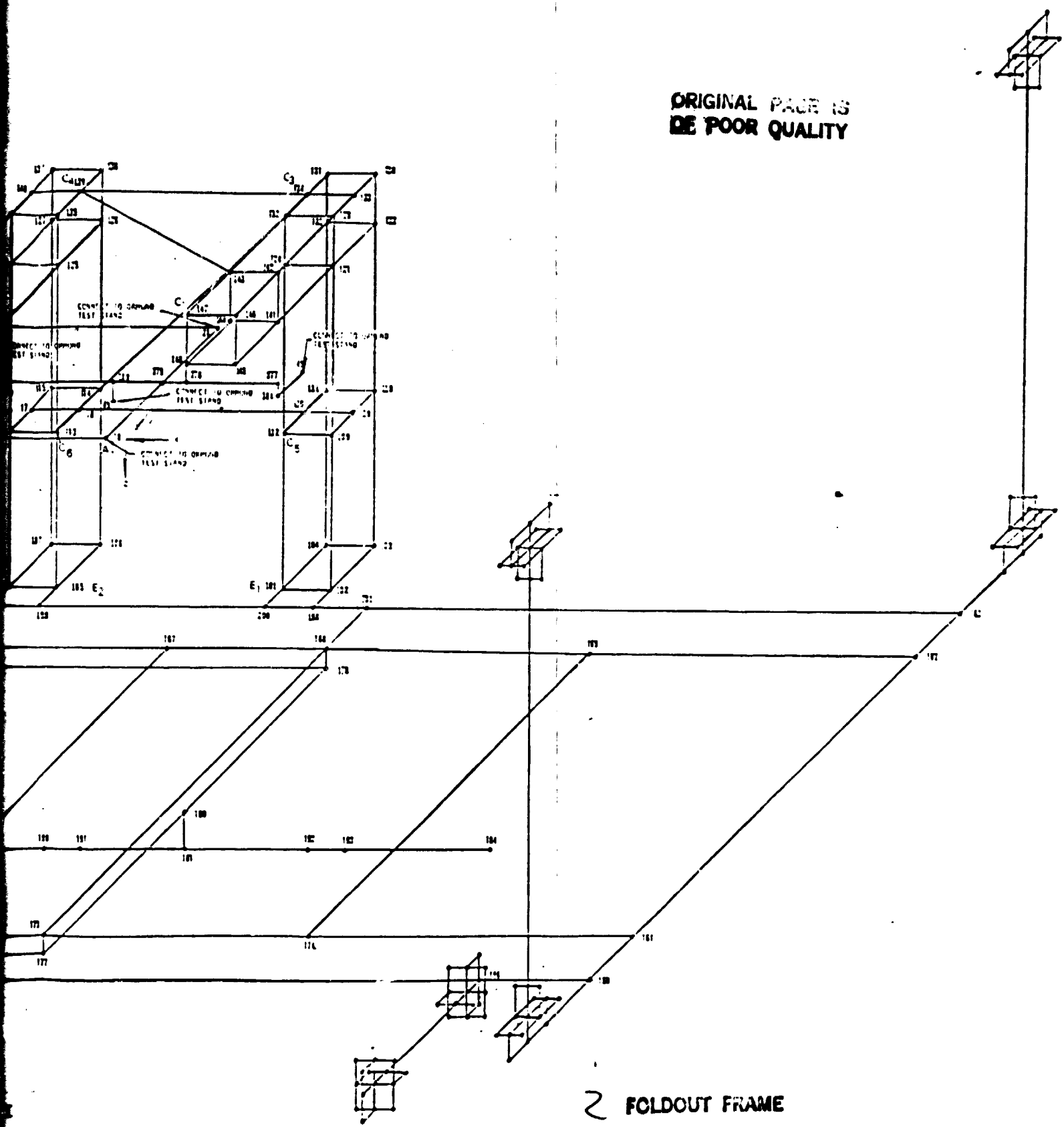

2 FOLDOUT FRAME

nodes and 379 elements and it utilizes the spaceframe library elements of the FINITE system. Assumptions are the same as previously explained for Model II. Nodes 183, 184, 194, 228-230, 236, 258, 259, 286-288, 315-317, 344-346, and 373-375 are fixed. Calibration loads, represented by nodal loads, are applied at two locations where the first load is applied at node 72, along the simulated engine centerline of the test stand, and the second load is applied at node 99, along the force line of the engine centerline calibration support frame.

3.0 RESULTS AND ANALYSIS

Models I, II, and III of Section 2 have been analyzed. Preliminary dynamic analysis considerations for test stands of this type are found in Section 4.

3.1 Model I Static Structural Analysis of the Ormond Test Stand (Component A) Subjected to Internal Calibration Loads Only

The Ormond test stand is designed with internal calibrators that apply known loads to verify proper operation prior to each test run. This allowed an analysis of the internal structure to be accomplished with minimum influence from the supporting structure of the stand. The results presented in this section point out possible internal interaction factors affecting test stand accuracy without considering external interaction factors of the attachment points.

The identification of internal interactions that cause cross-coupling effects (loads paths that find their way into other axes) between the two measuring axes of the Ormond test stand is done by application of finite element analyses to Model I. Possible causes of these interactions are:

1. The misalignment of the calibration loads and load cells.
2. The distortion due to deflection of structure underload.
3. The stiffness of flexures in bending and torsions.

The theoretical predictions of Model I are compared with experimental results obtained from the internal calibration conducted at NASA Lewis PSL facility. Two effects are found to be significant. They are the effects of the misalignment of the load cells and applied forces, and the effect of the stiffness of the test stand members and joints. The misalignment of the load

cells and applied forces was found to have the same effect as seen by computer simulation. Since the Ormond test stand has special design features to minimize misalignment effects of the load cell measuring axes, it is reasonable to assume that the misalignment effect is caused mainly by misalignment of the applied forces. In addition, it was found that the preload on the load cells with no forces applied to the test stand caused off-sets (biases) in the data. A systematic variation of the parameters of the model yielded insights into possible causes of coupling effects. The results are graphicaly represented in Figures 13 through 16 (following).

Figure 13 shows the analytical and experimental effect of side load applied at the forward load cell on the force measured at the forward sideward load cell. This figure represents the accuracy of the calibrator load cells. Both experimental and predicted data are shown. As should be expected, all simulated results passed through zero, where no force is applied and no force should be measured by the load cell. The linear fit of the experimental measurements shows a force under the zero load condition which indicates the existence of a slight preload on the load cell of 2.5 pounds. The effect of misalignments of zero and 1.0 degree are predicted to produce 9 (.18%) and 14.5 (.29%) pounds respectively in response to a 5,000 pound load. The effect of a ten percent reduction of stiffness for all the test stand members can produce a 16.0 (.32%) pound load in response to a 5,000 pound load.

Figure 14 shows the analytical and experimental effect of side load applied at the forward load cell on the force measured at the aft sideward load cell. The experimental measurements indicate a slight preload on the load cell of 1.5 pounds. The effect of misalignments of zero and .5 degrees are predicted to produce 5.0 (.10%) and 7.5 (.15%) pounds respectively in response to a 5,000 pound load. A ten percent reduction of stiffness for all the test stand members produce 6.0 (.12%) to 7.0 (.14%) pounds in response to a 5,000 pound load.

Figure 15 shows the analytical and experimental effect of side load applied at the forward load cell on the force measured axially. The effect of misalignments and reduction of stiffness can be read directly from the figure. It appears that the experimental curve could be duplicated by applied force misalignment of approximately 1.2 degrees or a certain combination of

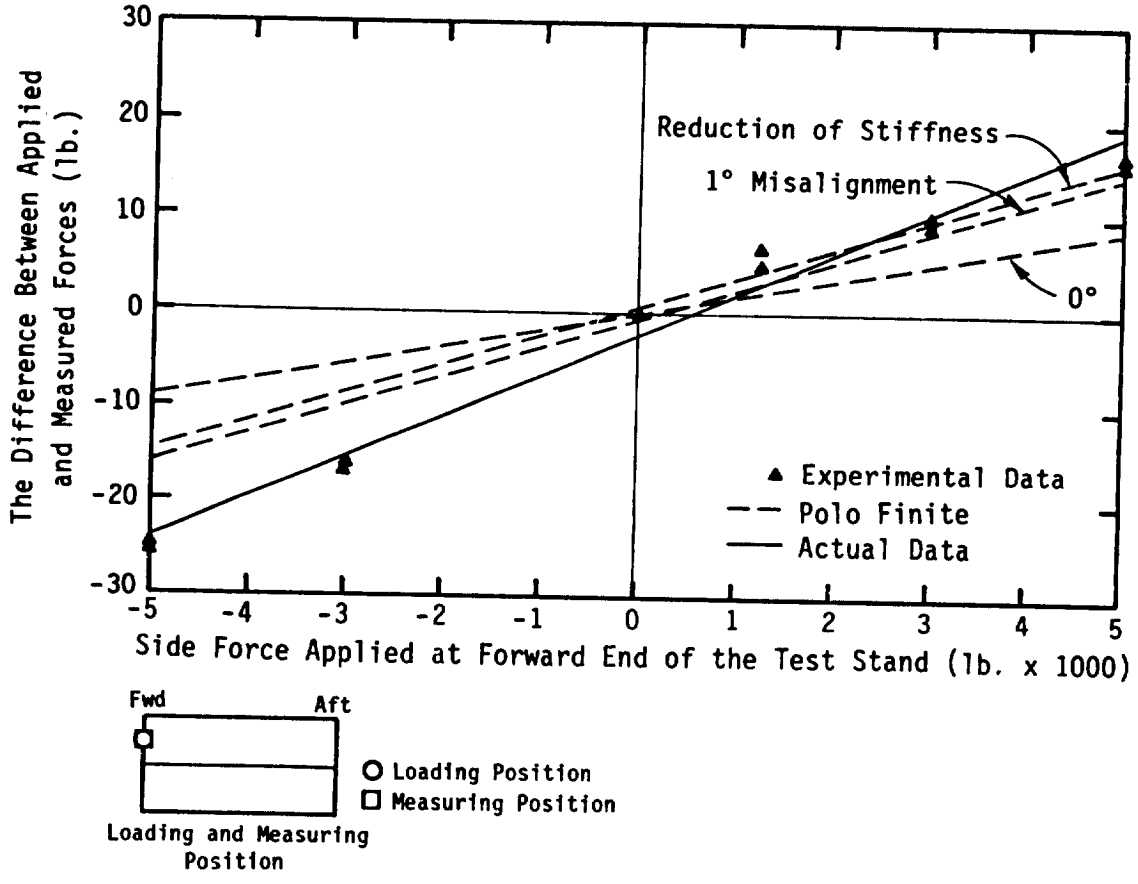

Figure 13. The Analytical and Experimental Effect of Side Load Applied at the Forward Load Cell on the Force Measured at Forward Sideward Load Cell

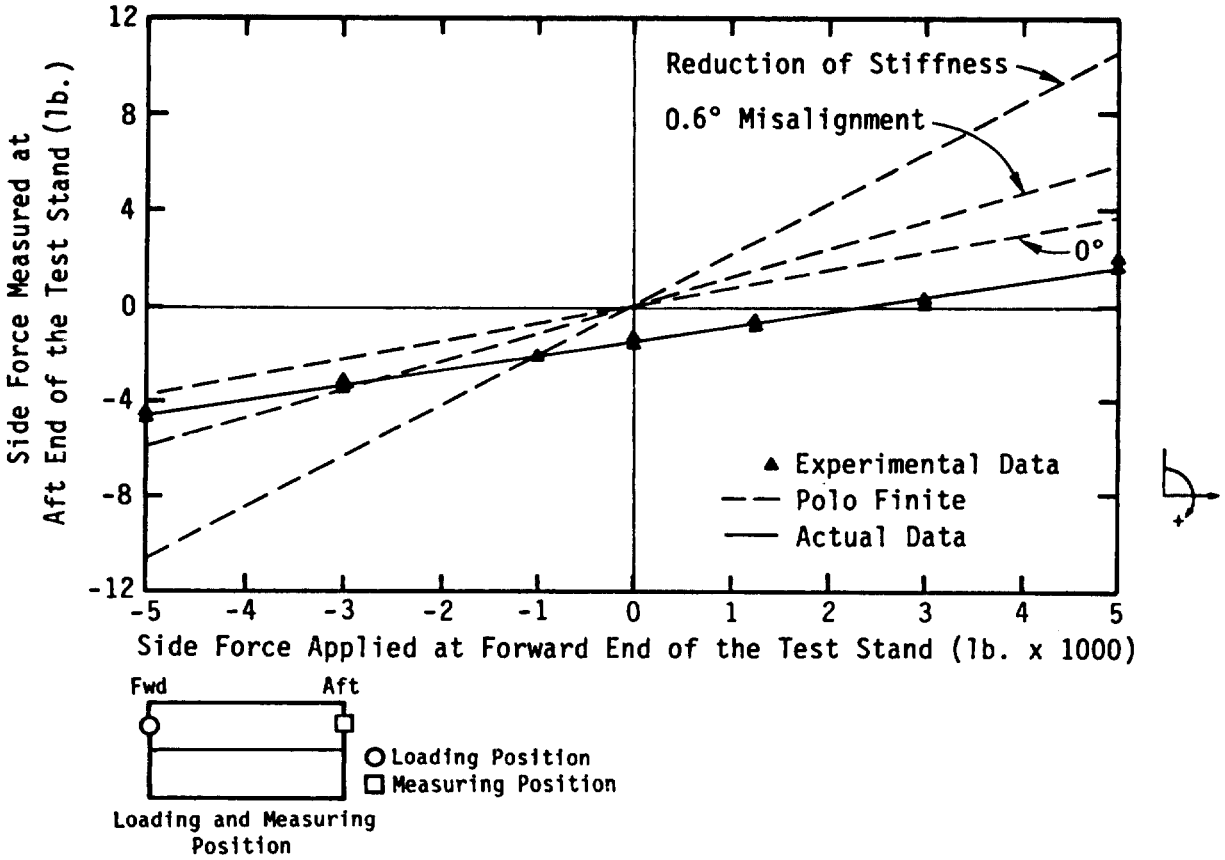

Figure 14. The Analytical and Experimental Effect of Side Load Applied at the Forward Load Cell on the Force Measured at the Aft Sideward Load Cell

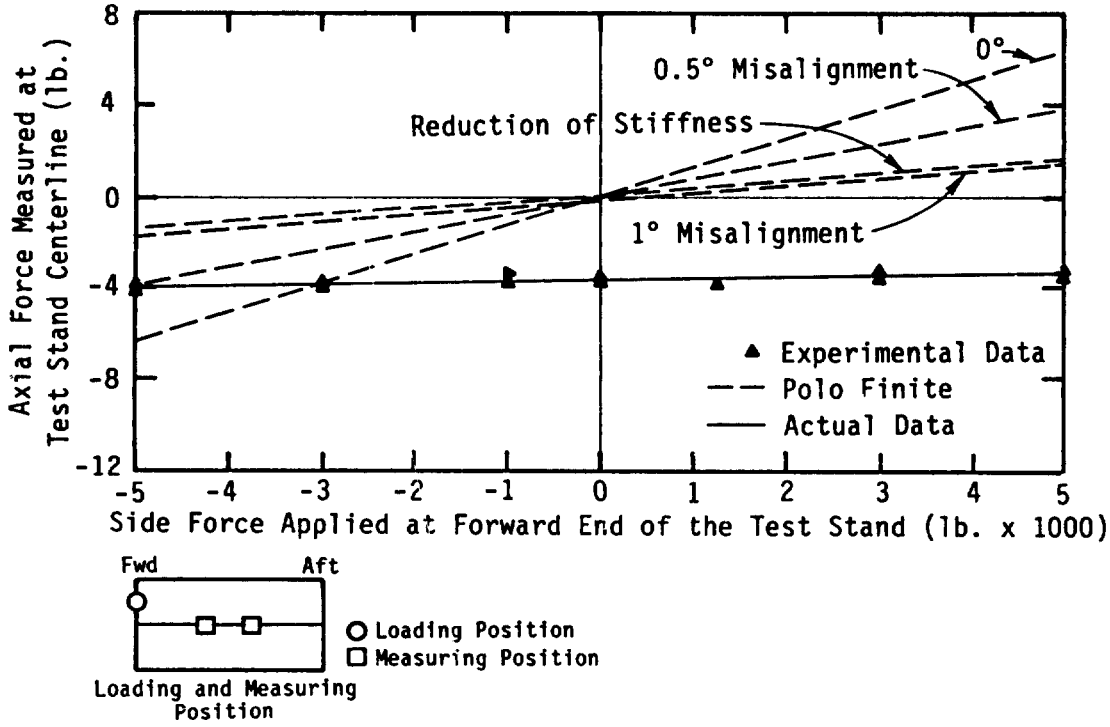

Figure 15. The Analytical and Experimental Effect of Side Load Applied at the Forward Load Cell on the Force Measured Axially

the applied force misalignment, reduction of test stand stiffness, and a 3.75 pound preload. Since low cross-coupling between axes is desirable for improvement of the test stand accuracy, this result should suggest that some intentional misalignment of the applied force could be beneficial in minimizing cross coupling. However, it should be emphasized that maximum coupling with no misalignment is expected to be approximately .12 percent. Reduced stiffness decreases the cross-coupling but is not recommended for design of test stands since it is not readily predictable for a normal operation. It could create undesirable inherent dynamic characteristics. The results explained cannot be regarded as unique until it is proven that the internal interaction is not the result of external interaction. An example would be the reduction of stiffness of the test stand support structure. Since the Ormond test stand was designed with very rigid and compact structural arrangements, the reduction of the model stiffness is not likely to be the prime factor creating a cross-coupling effect. External factors such as the weakness in the external calibration frame of PSL structures is a more probable cause of coupling effect. This factor will be further investigated in the next two sections.

Figure 16 shows the experimental and analytical effect of an axial load applied along the test stand centerline on the force measured at forward sideward load cell. The experimental result can be simulated by a combination of applied force misalignment of .5 degrees which produces about 5.0 pounds of cross-axis measurement, and a preload of 4.8 pounds. Note in this figure that when all the test stand stiffnesses is reduced by ten percent, there is no effect on cross-coupling. This further supports the conclusion that the structural weakness is caused by external sources (e.g., the support structure).

From prior information presented in this section, cross-axis sensitivities are less than .35%. There is more error in the internal calibrators themselves than in the cross-axis sensitivities. Experimental results can be expressed as the summation of the effects of internal preload, internal misalignment of calibrator force, and stiffness. Interaction due to internal stiffness of the Ormond test stand is less pronounced because the test stand is very rigid and compact. It appears that external structural weakness of either the external calibrators (components B and D of Figure 2) or the PSL

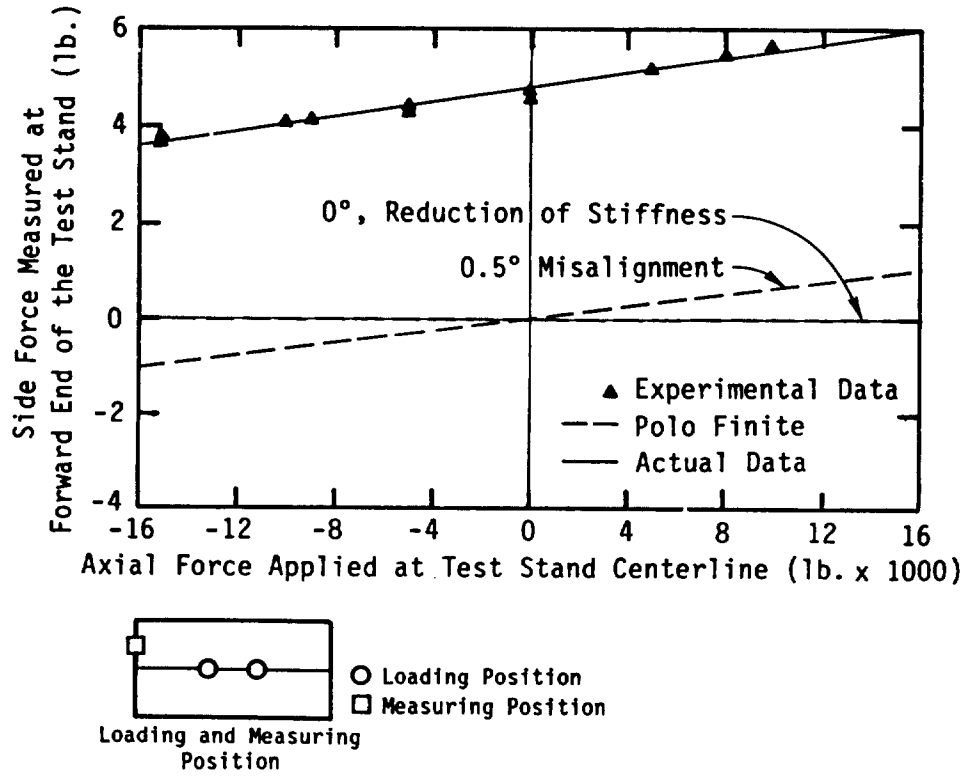

Figure 16. The Analytical and Experimental Effect of Axial Load Applied Along the Test Stand Centerline on the Force Measured at Forward Sideward Load Cell

structures (components C and E) caused the cross-axis measurement. The next two sections will investigate this hypothesis.

3.2 Model II Static Structural Analysis of the Ormond Test Stand with External Calibration Frame (Components A and B) to Simulate Loads Applied at the Engine Centerline

Model II adds to Model I the complexity of an external calibration frame (component B of Figure 2) which allows loads to be applied at the axis of the engine to be tested. This adds a possibility of amplified interactions and deflection due to stiffness of component B. The theoretical predictions of Model II are compared with external calibration results, and graphically represented in Figures 17 and 18. Both of these figures indicate almost no cross-coupling effect of a 10% reduction in component B stiffness, with the exception of interaction due to misalignment of applied force.

Figure 17 shows the experimental and analytical results of the effect of a side load applied at simulated engine centerline on the force measured axially. The resultant force measured axially is independent of applied lateral load when the lateral load is aligned properly (i.e., zero misalignment). Reduction of the external calibration frame stiffness by ten percent indicates a negligible (one pound in ten thousand) amount of cross-axis measurement. The experimental results show that approximately .6 percent of an applied external load is measured in the cross-axial axis. By simulation, an induced misalignment of applied force of .31 degree causes the prediction to agree with the experimental result. This is an indication that there is some misalignment in the calibration force. In addition, the experimental result passed through the origin indicating the absence of preload in the test stand. Similar results are found in Figure 18, which shows the experimental and analytical effect of axial load applied at simulated engine centerline on the force measured laterally. The experimental results show that the calibration force is not aligned. This is due to an indication that approximately .4 percent of the applied axial load is measured in the cross lateral axis, and .22 degree induced misalignment of the applied load causes the simulated and experimental results to agree. The experimental result shows no preload in the test stand.

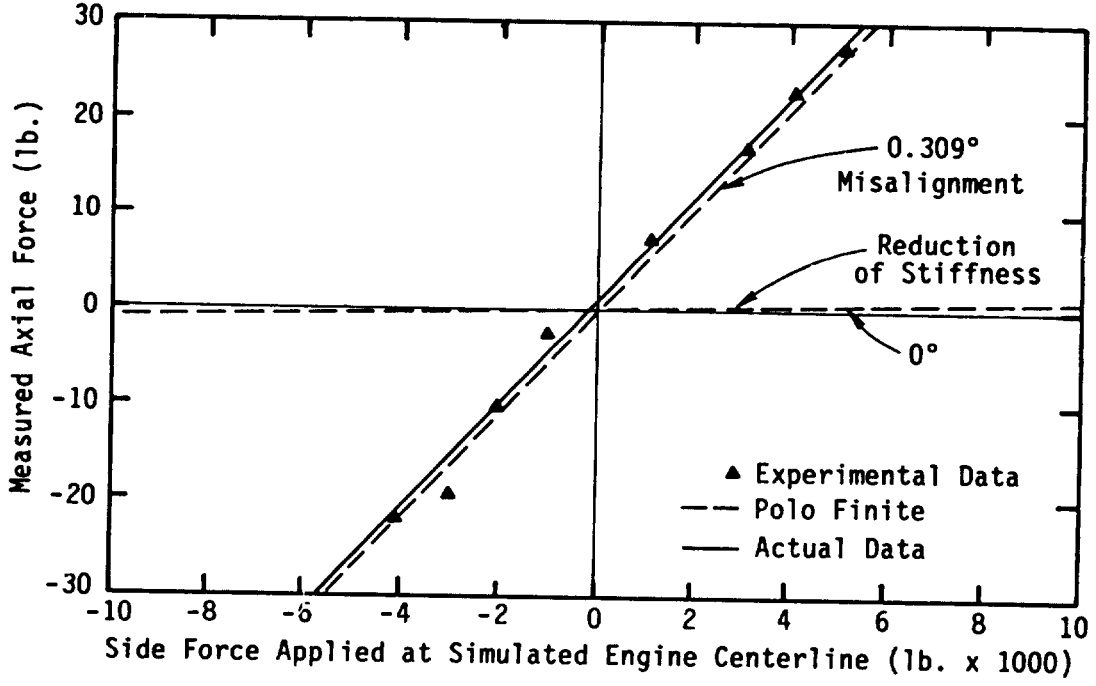

Figure 17. The Analytical and Experimental Effect of Side Load Applied at Simulated Engine Centerline on the Force Measured Axially

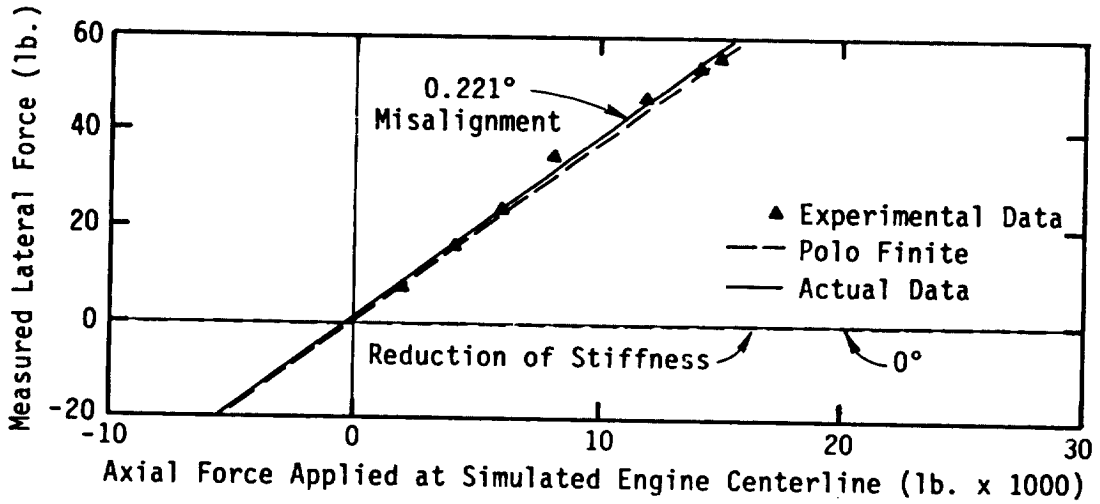

Figure 18. The Analytical and Experimental Effect of Axial Load Applied at Simulated Engine Centerline on the Force Measured Laterally

From this analysis, the following conclusions can be drawn:

1. The test stand appears to have been adjusted to eliminate the preload observed in section 3.1, because there is no indication of measured load when no load is applied.
2. The cross-coupling effect is usually caused by misalignment of the external calibrator force.
3. Reduction of calibration frame stiffness has no effect on cross-axis measurement.

Thus, any significant calibration errors must lie outside the Ormond test stand with engine centerline thrust simulation frame attached. An expanded analysis is the subject of the next section which involves the overall PSL facility.

3.3 Model III Static Structural Analysis of PSL Facility and the Ormond Test Stand Integration with the Engine Centerline Calibration Frame Installed (Components A, B, C, D, and E)

The previous analyses of Model I and II indicate minimal internal sources of error, and that misalignment of the calibration loads is being produced external to the system. A schematic of the entire supporting structure of the PSL is shown in Figure 2. Model III has been formulated to represent every component of this schematic except the supporting suspension flexures of the PSL. Component A is represented by Model I. The combination of components A and B represents Model II. The result of Model I analysis indicated that the Ormond test stand was affected by internal preload, internal misalignment of calibrator force, and stiffness. It was suggested that interaction due to internal stiffness of the test stand is not a large effect. A more probable cause of cross coupling would be the external stiffness caused by either the external calibrators (B and D) or PSL structures (C and E). The result of Model II analysis indicated the external misalignment of calibrator force as the main factor causing cross coupling. The reduction of the external calibration frame stiffness was caused by either the external calibrators (B and D) or PSL structures (C and E). The result of Model II analysis indicated the external misalignment of calibrator force as the main factor causing cross coupling. The reduction of the external calibration frame stiffness produced a negative effect. By deduction, from this discussion of results, it was evident that the weakness in one of components of the PSL structures influenced the experimental accuracy of the test stand. Supporting this conclusion was the result obtained during the external calibration process at the NASA PSL

facility where it was discovered that 10,000 pounds of external calibrator axial force applied to the calibration fixture caused an average displacement of about .375 inches between calibration fixtures B and D. This pointed to the PSL components as the cause of the deflection. To verify this, Model III was created to determine which PSL component caused the structural weakness. The first step was to use a completed version of Model III which considered components A, B, C, D, and E. Model III's loading simulation predicted an average displacement between calibration fixtures B and D of approximately .201 inches when subjected to 10,000 pounds axial force. Table 1 summarizes nodal displacements in response to 10,000 pounds of simulated axial load. The simulation results indicated negligible displacements of components D and E, which could be considered as rigid components of the PSL structures. This leaves component C, the supporting superstructure, as the probable cause of the deflection.

Model III was modified to keep components D and E fixed. This allowed the investigation to focus on only the structural characteristics of components A, B, and C. The same average displacement of .201 inches was found when 10,000 pounds axial load was applied to the calibration frame. Since previous analyses demonstrated A, B, D, and E to be quite rigid, it was concluded that component C caused the large average displacement and the cross-coupling misalignment effect indicated by the Model II analysis.

To verify this assertion, component C was isolated and analyzed separately. Response to loads of 10,000 pounds were applied to the upper parts of component C and at the attachment location of the Ormond test stand (component A). A large displacement of .193 inches was found in the component C upper structures. The displacement of component C lower structures was small and negligible.

NASA has taken steps to correct this problem by reinforcing the component C upper structure. A similar modification was made to the component C model and the analysis was repeated using the same simulation load. A reduction in the average displacement was reduced to .02 inches which represents about ten percent of the unmodified value.

Table 1. Model III - Nodal Displacements for 10,000 Pounds of Simulated Axial Load

Node	Displacement, in. x	y
0	0.0000	0.0000
A1	-0.2012	0.0961
A2	-0.2012	0.0200
C1	-0.1788	0.1183
C2	-0.1517	0.0667
C3	-0.1116	0.1184
C4	-0.1117	0.0668
C5	-0.0600	0.0525
C6	-0.0598	0.0331
E1	-0.0019	0.0021
E2	-0.0022	0.0021
E3	0.0011	0.0031
E4	0.0071	0.0033
D1	0.0183	0.0044
D2	0.0155	-0.0007

Note: Node positions can be found in Figure 12.

3.4 Summary of Finite Element Analysis

In summary, Model I, II, and III analyses have shown that the finite element modeling technique is an effective way to evaluate and identify inherent problems within the design. It has successfully verified experimental results. If it had been applied during the design phase, the developmental problems could have been identified and averted.

The "Spaceframe" model is capable of representing the characteristics of a multi-component test stand. Problems were identified and solutions were suggested by comparing the computer simulated and experimental results. The accuracy of the Ormond test stand was found to be affected most by misalignment of the applied force. Cross-axis measurement caused by the misalignment can be eliminated either by intentionally inducing misalignment of the applied force to coincide with misalignment angle, or by using calibration correction coefficients. The weakness in the upper PSL engine mount structure was identified as the major element affecting test stand accuracy. It was corrected by reinforcing the structure.

4.0 DYNAMIC CONSIDERATION OF THE ORMOND TEST STAND

While finite element analysis has shown its value in static analysis, it is of little use in the study of the dynamics of test stand to time variant thrust vectoring.

The dynamic analysis in this section is a simplified preliminary investigation of possible mathematical models for analyzing the dynamic response characteristic of the test stand load cells to rapidly changing forces (Ref. 9). No experimental data were available with which to compare these results. Three damping models were considered. The first was a baseline second-order linearly damped system; the second was a non-linearly damped system with free vibration; and the third was a Coulomb-friction-damped free vibration system.

Several assumptions were made regarding mathematical models for all systems. The dynamic analysis was based on single degree-of-freedom (SDOF) system which allowed displacement in only one direction. A simple spring-mass system was considered where the spring constant was the load cell stiffness and the pendulom mass was considered as consisting of a selected weight of the

engine and one-half of the Ormond test stand weight. The spring constant of the load cell was 30 x 105 lb/in and the mass selected was 155.28 lb-sec^2 /in for all of the following analyses.

4.1 Linear Viscous Damping

The response of load cell for viscous-damped SDOF system subjected to ideal step input was mathematically represented by a second order linear differential equation of the form mu+cu+ku = P(t). An ideal step input of 1000 pounds was used. The general solution to the equation is:

$$u(t) = \frac{P_o}{k} \; 1-e^{-\xi W_n t} \left(\cos W_d t + \left(\frac{\xi W_n}{W_d}\right) \sin W_d t\right)$$

where u(t) = load cell displacement
k = load cell displacement
ξ = viscous damping factor
t = time
W_n = natural frequency = 139.0 rad/sec
W_d = damped frequency = $W_n (1-\xi^2)^{1/2}$
F_o = 1000 lb ideal step input

The solution was calculated at various damping ratios between .03 and .80. The results are graphically presented in Figures 19, 20, and 21. The figures show the exponential decoy of amplitude with time. This, the most commonly used engineering model for dynamic problems can serve as a basis for comparing other models.

4.2 Non-Linear Damping

The non-linear dynamic response of the load cell is assumed to be affected by the aerodynamic damping force. This drag force is a function of velocity squared, which can be expressed as:

$$D = 1/2 \, \rho v^2 S C_d,$$

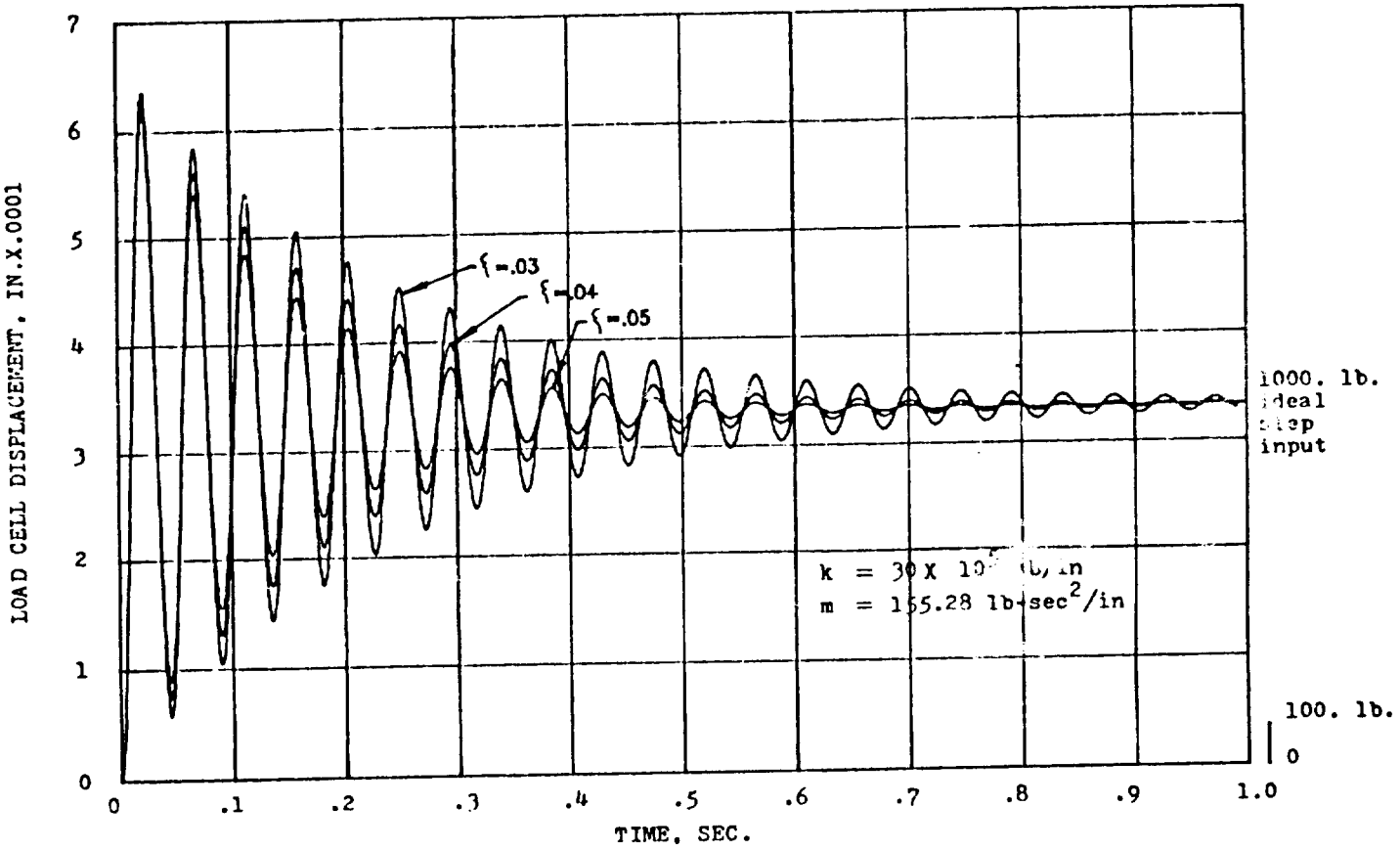

Figure 19. Linear Dynamic Response of the Load Cell When Subjected to Ideal Step Input of 1,000 Pounds for Lowly Viscous Damped Spring Mass System

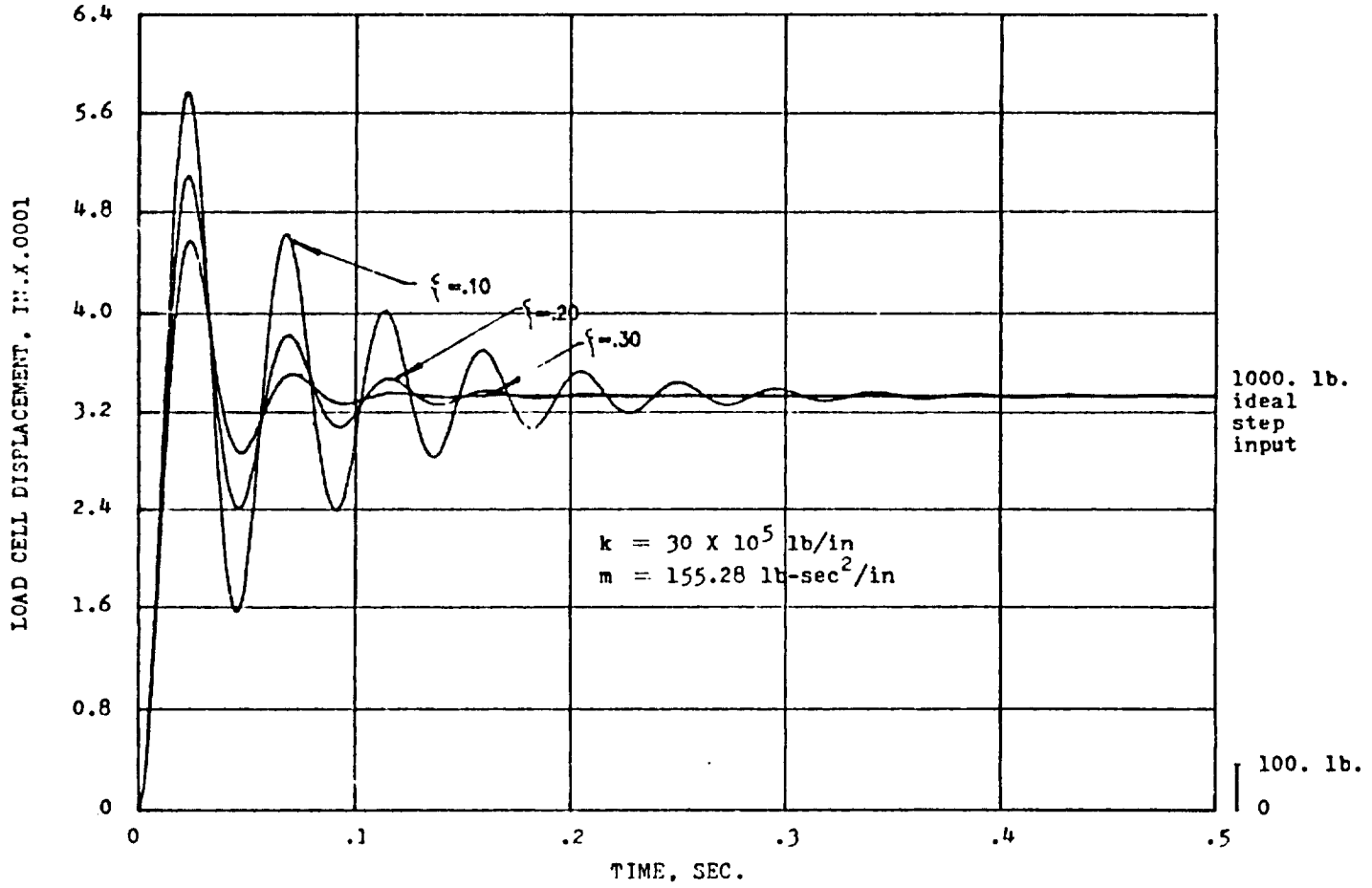

Figure 20. Linear Dynamic Response of the Load Cell When Subjected to Ideal Step Input of 1,000 Pounds for Slightly Viscous [illegible]pring Mass System

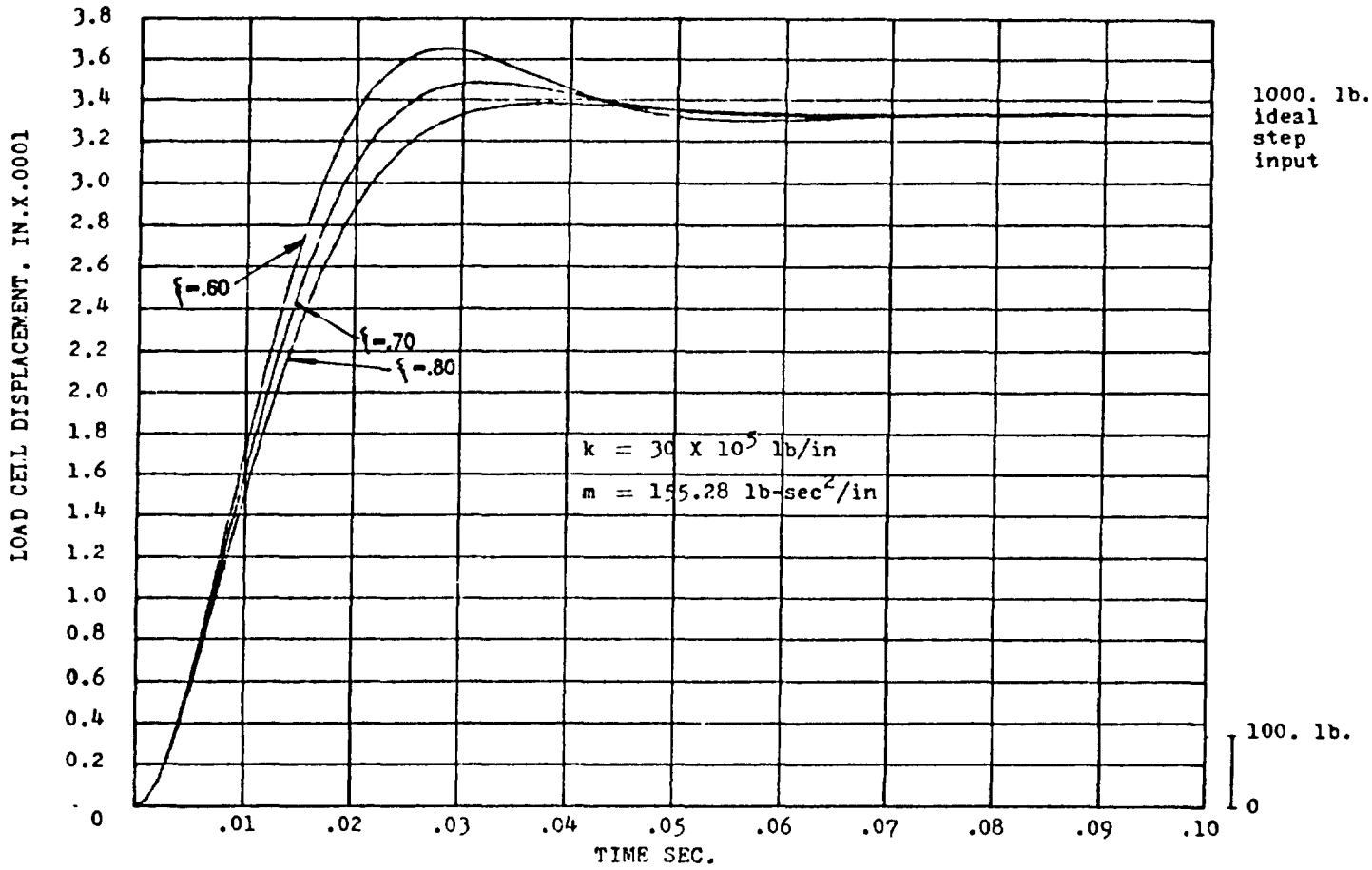

Figure 21. Linear Dynamic Response of the Load Cell When Subjected to Ideal Step Input of 1,000 Pounds for Near Optimally Viscous Damped Spring Mass System

where ρ = air density

v = velocity relative to the air

C_d = drag coefficient

S = test stand reference area

Assuming all the above parameters except the velocity to be constant the potential for non-linear response of the test stand is evident. The general equation of motion for the SDOF system, free vibration with viscous and aerodynamic dampings, can be mathematically represented as $mu+C_d(u)^2+cu+ku=P(t)$, where P(t) is zero for free vibration. There is no closed-form solution to this equation because of the non-linearity induced by velocity squared term. The solution can be obtained either by numerical integration or by a method of approximation to a closed-form solution (Ref. 10). Since this study was preliminary, an approximation to a closed-form solution developed by Krylotr and Bayainloff (KB) was used. The KB approximation method applies to the equation of motion where the velocity is slowly varying. The solution found by the KB method for free vibration is expressed as $u(t) = \frac{u_o}{\cos A} \cos(W_n(1-\xi^2)^{1/2} t+A)$, where u_o = initial displacement

= 3.333 x 10 in. (100 lb t<0, 0 lb t>0]

$$A = \tan^{-1}\left(\frac{-\xi}{(1-\xi^2)^{1/2}}\right)$$

The other variable definitions are the same as for the linear equation. Various damping ratios between .03 and .30 were used in the calculation and are graphically presented in Figures 22 and 23. The reponses are quite similar to those obtained for the simple second order system. Only when they are overlayed can the differences be seen.

4.3 Coulomb Damping

Coulomb, or dry-friction damping, is represented by the sliding friction force created by a mass sliding on a rough surface. Since friction force always opposes the motion (i.e., its direction is opposite to that of displacement (u)), the equation of motion for a SDOF, free vibration with Coulomb damping, can be represented mathematically by:

$$\ddot{u} + W_n^2 u = -W_n^2 u_d, \dot{u} \neq 0$$

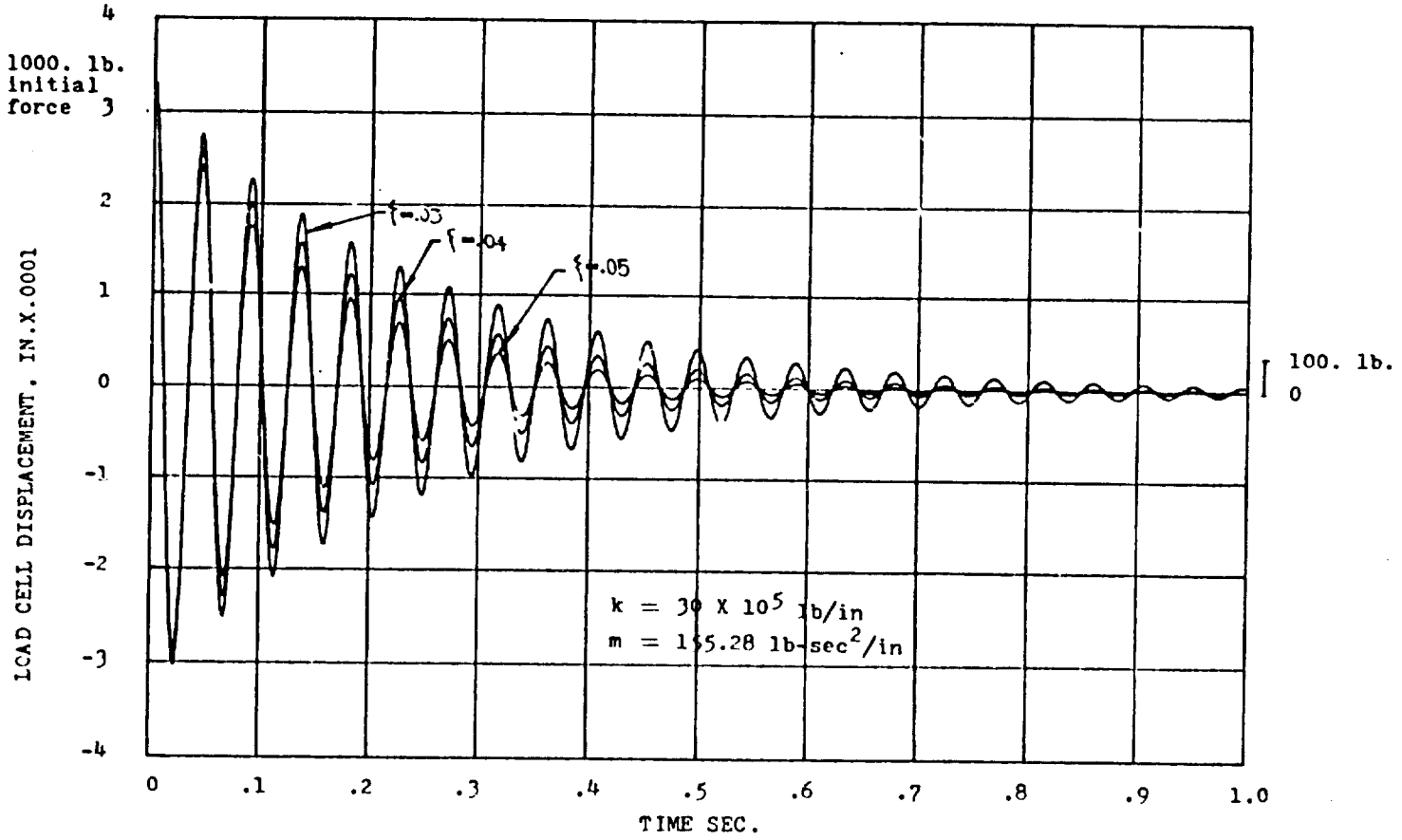

Figure 22. Non-Linear Dynamic Response of the Load Cell for Lowly Damped Free Vibration Spring Mass System

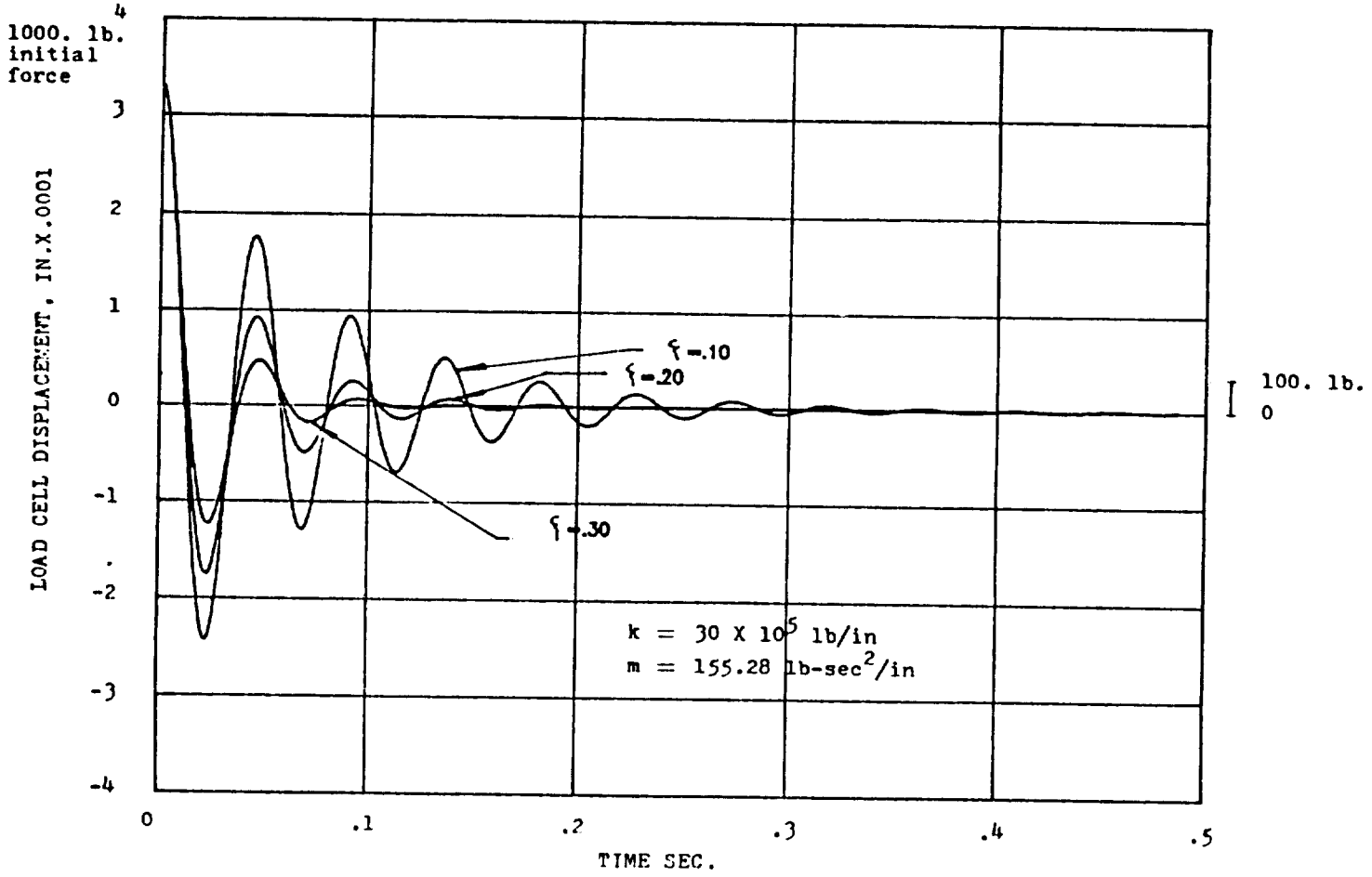

Figure 23. Non-Linear Dynamic Response of the Load Cell for Highly Damped Free Vibration Spring Mass System

$$\ddot{u} + W_n^2 u = + W_n^2 \mu_d,$$

where μ_k = coefficient of kinetic friction

u = the displacement

$$\mu_d = \frac{\mu_{kg}}{W_n^2}$$

The equation of motion with Coulomb damping depends on the rate of change of velocity u. The general solution to the equation of motion is

$$u(t) = (u_o - \frac{g}{W_n^2}\mu_k) \cos W_{nt} + \frac{g}{W_n^2}\mu_k), \quad u > 0$$

$$= (u_o + \frac{g}{W_n^2}\mu_k) \cos W_{nt} + \frac{g}{W_n^2}\mu_k), \quad u < 0$$

It was found from the testing of the Ormond test stand that the coefficient of kinetic friction was very small. This observation led to the selection of small coefficients: .005, .075, and .010 are examples. The resulting motions were calculated by a computer program and are plotted in Figure 24. Note that the Coulomb damped system behaves like an undamped SDOF system whose equilibrium position is shifted at the end of each half-cycle. A distinguishing feature of that response is that amplitude decays linearly with time rather than exponentially as for viscously damped systems.

4.4 Comparison of the Dynamic Analyses

The effects of linear, non-linear, and Coulomb damping on the amplitude decay characteristic are graphically summarized in Figure 25. The Figure shows the relationship between damping ratio and time to reach one-tenth amplitude. The time to reach one-tenth amplitude for linear and non-linear systems increases somewhat exponentially as the damping factor decreases. The time to reach .10 amplitude is not the same for each model. The effect of damping characteristics on the number of cycles to reach 1/10 amplitude is shown in Figure 26. Coulomb damping appears to be the most effective means of damping the system. However, stiction may cause problems with the systems returning to the same zero point following each disturbance.

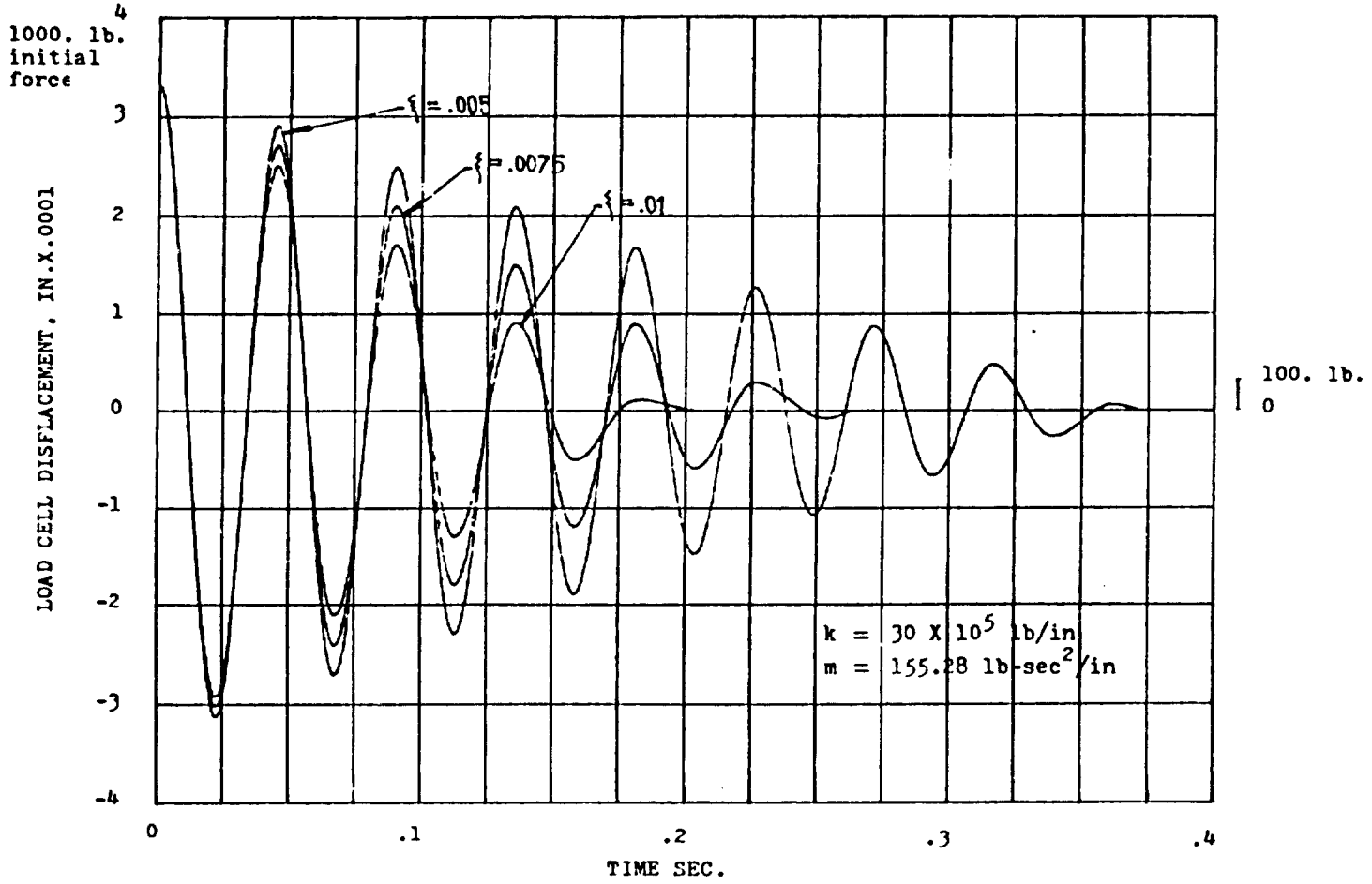

Figure 24. Dynamic Response of the Load Cell for Coulomb Damped Free Vibration Spring Mass System

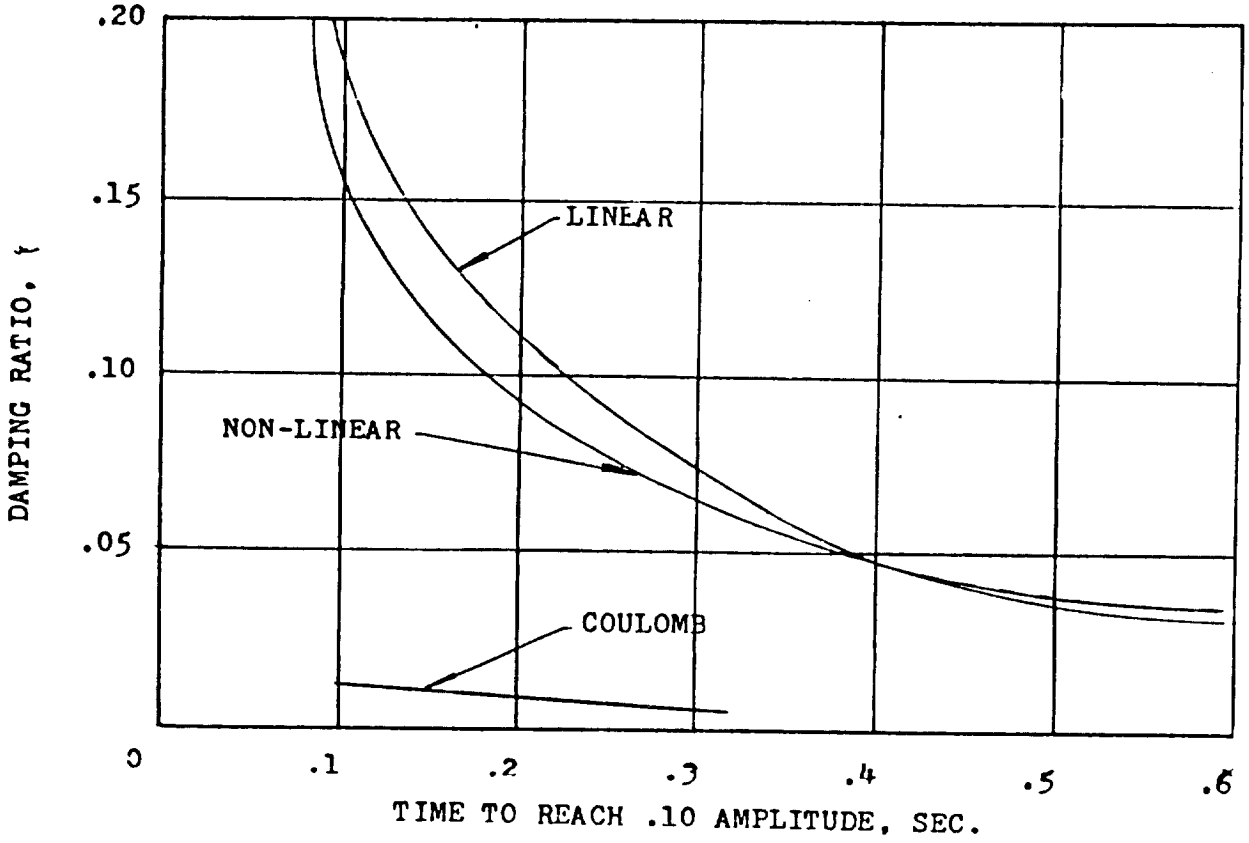

Figure 25. The Effect of Damping Ratio on the Time to Reach .10 Amplitude

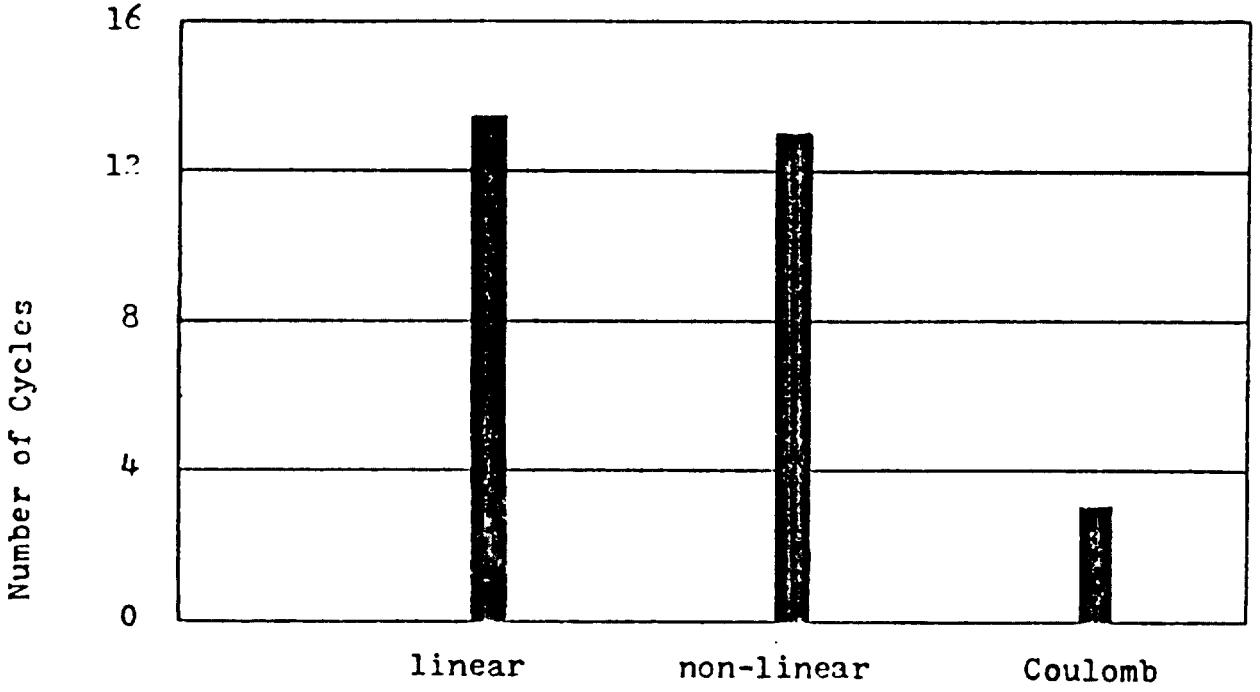

Figure 26. The Effect of Damping Characteristic on the Number to Cycles to Reach .10 Amplitude

While this is a preliminary study, it indicates the different types of applicable mathematical models. The result of this study can be used as an initial step toward a more detailed study. It should be considered that the damping of a real system usually results from looseness of joints, internal damping in the material and therefore is not ideal. However, if the decay vibration characteristic is found, it may be assumed that viscous, aerodynamic, or Coulomb damping can be used in the mathematical model system depending on how rapidly the oscillation must be damped. Some combination of Coulomb and viscous damping may be in order. That is, Coulomb damping is used for the large amplitudes and is switched out at the low, thus eliminating the non-return to zero objection for Coulomb damping.

5.0 CONCLUSIONS

A finite element (POLO-FINITE) analysis has been successfully applied to a multi-axis thrust measurement apparatus installed in the NASA Lewis Propulsion Simulation Laboratory (PSL). This analysis has been verified by comparing with experimental data, thus validating its use as an analytical tool to evaluate multi-component test stands for vectored thrust airbreathing jet engines. Interaction problems were identified. Factors affecting multi-component test stand accuracy originated from the following:

(1) internal preload
(2) internal calibration force
(3) external calibration force
(4) attachment of the test stand to the PSL engine mount structure

These problems were found from analysis of three separate models. The problem on internal preload can be removed by adjusting the load cells. Interactions due to misalignment of internal and external calibration forces can be minimized either by intentionally inducing misalignment to coincide with the measuring axis, by applying calibration correction coefficients, or by designing engine mount structures strong enough to resist and minimize displacement.

A separate dynamic analysis of the test stand was done using traditional manual methods. This study showed several means of damping the test stand during thrust vectoring operations. Of the three evaluated, Coulomb damping appears to be the most effective and to offer the greatest promise if it can

be incorporated without inducing sticktion or other adverse effects. A more detailed study is required to make these approaches truly useful in designing test stands that can measure the thrust components of vectored thrust jet engine.

It is recommended that these tools be employed to design and develop a protype for a six-component test stand for airbreathing vectored thrust engines. This work has shown that it can be done with great assurances of success.

REFERENCES

1. Schweikhard, William G., Peterson, Duayne, Killingswroth, Russel, Survey of Open Literature Concerning Multi-axis Thrust Measurements, University of Kansas, Lawrence, Kansas, April, 1981.

2. User's Guide to the POLO-FINITE System on the Honeywell Computer System, Academic Computer Center, University of Kansas, Lawrence, Kansas, August, 1979.

3. Lopez, Leonard A., Dodds, Robert H. Jr., Rehak, Danial R., Urzua, Jorge, POLO-FINITE, Department of Civil Engineering and the Academic Computer Center, University of Kansas, Lawrence, Kansas.

4. Popov, E.P., Mechanics of Materials, 2nd edition, Prentice-Hall Inc., Englewood, New Jersey, 1976.

5. Zienkiewicz, O.C., The Finite Element Method, 3rd Edition McGraw-Hill Book Company (UK) Limited, London, 1977.

6. Ormond, A.N., "Measurements, Instrumentation, Automation", Ormond, Inc., Santa Fe Springs, California.

7. Example Problems Manual for POLO-FINITE Structural Mechanics System, Department of Civil Engineering, University of Illinois, Urbana-Champaign and Department of Civil Engineering, University of Kansas.

8. Singnoi, Werochane N., Evaluation of POLO-FINITE Modeling as a Design and Analytical Tool for Multi-Component Vectored thrust Jet Engine Test and, University of Kansas Masters thesis, June 1985.

9. Craig, Roy R. Jr., Structural Dynamics, John Wiley & Sons, Inc., New York, 1981.

10. Beecham, L.J., Titchener, I.M., "Notes on an Approximate Solution for the Free Oscillation Characteristics of Non-Linear Systems Typified by $x + Fcx, \dot{x} = 0$", British Aeronautical Research Council, R & M No. 3651, August, 1969.